Néel temperature and reentrant H-T phase diagram of quasi-two-dimensional frustrated magnets

Burkhard Schmidt and Peter Thalmeier
Max Planck Institute for the Chemical Physics of Solids, 01187 Dresden, Germany
(Received 25 September 2017; revised manuscript received 14 December 2017; published 29 December 2017)

In quasi-two-dimensional (quasi-2D) quantum magnets, the ratio of Néel temperature T_N to Curie-Weiss temperature Θ_{CW} is frequently used as an empirical criterion to judge the strength of frustration. In this work, we investigate how these quantities are related in the canonical quasi-2D frustrated square or triangular J_1-J_2 model. Using the self-consistent Tyablikov approach for calculating T_N we show their dependence on the frustration control parameter J_2/J_1 in the whole Néel and columnar antiferromagnetic phase region. We also discuss approximate analytical results. In addition, the field dependence of $T_N(H)$ and the associated possible reentrance behavior of the ordered moment due to quantum fluctuations are investigated. These results are directly applicable to a class of quasi-2D oxovanadate antiferromagnets. We give clear criteria to judge under which conditions the empirical frustration ratio $f = \Theta_{CW}/T_N$ may be used as measure of frustration strength in the quasi-2D quantum magnets.

DOI: 10.1103/PhysRevB.96.214443

I. INTRODUCTION

Long-range magnetic order is prevented at finite temperature in strictly two-dimensional (2D) spin systems with a continuous symmetry [1]. Commonly, the susceptibility would not have a singular cusp at a finite temperature but shows a broad maximum at a temperature that corresponds roughly to the average energy scale J_c of the intraplane exchange interactions. This behavior is indeed found experimentally in quasi-2D magnets and is also obtained theoretically using, e. g., finite-temperature Lanczos method (FTLM) based on exact diagonalization of finite clusters [2,3]. However, in reality these magnets nevertheless mostly exhibit long-range magnetic order at even lower temperature. This is due to their quasi-2D character caused by the finite interplane interactions $J_\perp \ll J_c$ in real compounds such as the $S = \frac{1}{2}$ layered vanadium compounds [4–7] listed in Table II. A famous example is La_2CuO_4, the antiferromagnetic parent compound of high-T_c superconductors. Although the interplane coupling is extremely small $J_\perp/J_c \approx 1.3 \times 10^{-6}$ a large Néel temperature $T_N = 325$ K is observed [8]. This is due to the fact that in quasi-2D magnets the ordering temperature is still determined by the large intraplane exchange ($J_c \approx 116$ meV) and is only logarithmically suppressed roughly by the factor $\ln(J_c/J_\perp)$. The physical reason is that a strictly 2D Heisenberg system is at a quantum critical point with algebraic decay of long-range correlations. Then, even tiny interlayer coupling may lead to sizable 3D ordering temperature [9].

This matter is well understood in the nearest-neighbor (NN) Heisenberg antiferromagnet and has been quantitatively investigated with numerical Monte Carlo (MC) simulations [10] and approximate theories based on Tyablikov random phase approximation (RPA theory) [9,11–13] and also more advanced analytical methods [14–17]. On the other hand, the restriction to only NN interactions which are furthermore isotropic in the lattice misses a large body of known frustrated quasi-2D magnets that are described by the square lattice J_1-J_2 model or the related anisotropic triangular J_1-J_2 models (Fig. 1). In these systems, the general behavior of the ordering temperature $T_N(\phi, J_\perp)$ as function of frustration control parameter $\phi = \tan^{-1}(J_2/J_1)$ has not been investigated systematically in the two possible Néel (NAF) and columnar (CAF) antiferromagnetic regions (inset of Fig. 2) but in the frustrated ferromagnetic (FM) case [18]. In the interior of the AF phase regions it is well understood how the ordered moment reduction at zero temperature depends on ϕ, e.g., from linear spin wave theory (LSW) and comparison with exact diagonalization (ED) results [19,20]. The ordered moment is determined by the interplay of quantum fluctuations and frustration and may be completely suppressed on approaching small intervals of ϕ or J_2/J_1 around the classical phase boundaries where a spin liquid state or more exotic order is expected and LSW breaks down. The frustration dependence of the ordered moment will lead to a concomitant dependence of the overall energy scale of spin excitations. Consequently, the quasi-2D finite Néel temperature should show similar strong dependence on the degree of frustration. This is often empirically characterized by a "frustration ratio" $f = \Theta_{CW}/T_N$ where Θ_{CW} is the Curie-Weiss temperature. This ratio is expected to become large in the strongly frustrated regime where magnetic order breaks down and T_N vanishes. This may, however, not be the only possible origin for a large f value. On the other hand, it is also useful to define a microscopic frustration ratio $\kappa(\phi)$ which characterizes how far the ground-state energy of fundamental frustrated square and triangular tiles is increased with respect to their unfrustrated constituents.

It is the purpose of this work to clarify the connection between the quantities characterizing the frustrated magnet ground state and its finite-temperature behavior. In particular, we discuss how the size of the interlayer coupling $J_\perp$ can be estimated from the experimentally determined values of T_N and J_1, J_2. This is of great practical importance for frustrated magnets and we show how this may be achieved for the well-investigated oxovanadate layered compounds. For this purpose, we use the simple analytical Tjablikov theory which is based on a self-consistently scaled spin-wave dispersion. We extend this approach to calculate the field dependence of T_N which may be nonmonotonic due to the field-induced suppression of quantum fluctuations. Accordingly, a reentrant behavior for the ordered moment and a reentrant H-T phase diagram may be derived and we discuss a realistic example.

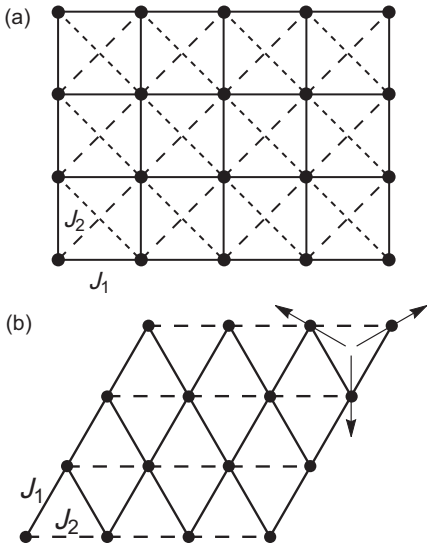

FIG. 1. J_1-J_2 exchange models on the square (a) or anisotropic triangular (b) lattices. In (b) the spin configuration of the maximally frustrated 120° structure (△) is indicated. In (a) J_1 and J_2 denote isotropic NN and NNN interactions, in (b) they denote bond-anisotropic NN interactions.

II. SQUARE AND ANISOTROPIC TRIANGULAR FRUSTRATED EXCHANGE MODELS AND THEIR CLASSICAL AND QUANTUM PHASES

These models provide a most instructive insight into the essentials of frustrated magnetism [20]. Furthermore, numerous realizations in magnetic compounds exist that allow for a comparison of theoretical to experimental results. Here, we employ the generic Heisenberg J_1-J_2 exchange model for both lattices as illustrated in Fig. 1 [21]:

$$\mathscr{H}_{\rm ex} = J_1 \sum_{\langle ij\rangle_1} \mathbf{S}_i \cdot \mathbf{S}_j + J_2 \sum_{\langle ij\rangle_2} \mathbf{S}_i \cdot \mathbf{S}_j. \tag{1}$$

It has the attractive property of having just one control parameter, the frustration ratio J_2/J_1, which allows to tune through a rich phase diagram in both cases. It is convenient to use a polar parametrization of the model which maps to a control parameter $\phi \in [-\pi,\pi]$ in a compact interval according to

$$J_1 = J_{\rm c}\cos\phi, \quad J_2 = J_{\rm c}\sin\phi,$$
$$J_{\rm c} = \sqrt{J_1^2 + J_2^2}, \quad \phi = \tan^{-1}\left(\frac{J_2}{J_1}\right). \tag{2}$$

We note that the anisotropic triangular model of Fig. 1(b) can be obtained from (a) by tilting the lattice and cutting one of the diagonal J_2 exchange bonds. Therefore, while (a) is an interaction frustrated model with NN and next-nearest-neighbor (NNN) bonds, (b) is a geometrically frustrated model with only (real-space anisotropic) NN bonds. The classical phase diagram is obtained from the minimum of the classical ground-state energy $E_{\rm cl} = NS^2 J_{\mathbf{Q}}$ where $\mathbf{Q}$ is the magnetic ordering vector and the exchange function is given by

$$J_{\mathbf{k}} = \begin{cases} \boxtimes : J_1(\cos k_x + \cos k_y) + 2J_2 \cos k_x \cos k_y + J_\perp \cos k_z, \\ \triangle : 2J_1 \cos\frac{1}{2}k_x \cos\frac{\sqrt{3}}{2}k_y + J_2 \cos k_x + J_\perp \cos k_z \end{cases} \tag{3}$$

for square (⊠) and triangular (△) lattices, respectively. The symbols for the special cases of the J_1-J_2 exchange model are defined in Table I.

Here, we included already the small AF coupling $J_\perp > 0$ between the 2D layers which are placed on top of each other to mimic the quasi-2D magnetism of real compounds. The moments are then staggered perpendicular to the 2D planes such that $Q_z = \pi$ for the 3D ordering vector $\mathbf{Q} = (Q_x, Q_y, Q_z)$. Three classical in-plane 2D phases ($J_\perp = 0$) occur in the same regions of ϕ for square and triangular lattices: ferromagnetic (FM) for $\phi \in [0.85\pi, -0.5\pi]$ with $(Q_x, Q_y) = (0,0)$, Néel antiferromagnet (NAF) for $\phi \in [-0.5\pi, 0.15\pi]$ with $(Q_x, Q_y) = (\pi,\pi)$ and for $\phi \in [0.15\pi, 0.85\pi]$ either a columnar antiferromagnet (CAF) for square lattice with $(Q_x, Q_y) = (\pi, 0)$, $(Q_x, Q_y) = (0,\pi)$ or a spiral phase (SPI) for triangular lattice with (Q_x, Q_y) varying continuously as function of ϕ between NAF and FM cases [22].

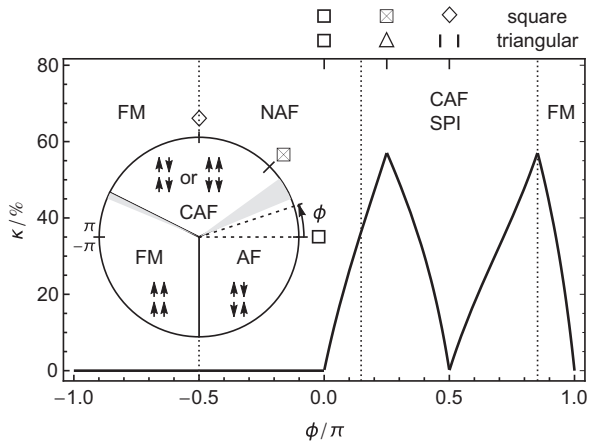

FIG. 2. Frustration degree of J_1-J_2 model in percent [Eq. (11)]. The maximum appears for $J_1 = J_2$ and at CAF(SPI)/NAF phase boundary. Here and in the following figures, the symbols on top are defined in Table I. Inset: classical phase diagram of square and anisotropic triangular J_1-J_2 models in polar presentation ($-\pi \leqslant \phi \leqslant \pi$, $J_{\rm c} = 1$). The CAF phase is twofold degenerate (a,b). For the triangular model it is replaced by the generally incommensurate spiral (SPI) phase.

TABLE I. Definition of symbols for general and special exchange models for square (top three) and triangular lattice (bottom four).

Symbol	Exchange	ϕ/π	Model
⊠	J_1, J_2	Any	General frustrated model
□	$J_2 = 0$	0	Pure Néel, latt. const. a
◇	$J_1 = 0$	$\pi/2$	Pure Néel, latt. const. $\sqrt{2}a$
△	J_1, J_2	Any	Anisotropic triangular
△	$J_1 = J_2$	$\pi/4$	Isotropic triangular
□	$J_2 = 0$	0	Pure Néel, latt. const. a
‖	$J_1 = 0$	$\pi/2$	Decoupled 1D AF chains

The classical ordered moment $m_{\mathbf{Q}} = S$ is only realized in the FM phase. In the AF or SPI phases, quantum fluctuations strongly reduce the moment, depending on the size of the spin S and frustration control parameter ϕ [22]. This may be concluded from linear spin wave (LSW) [2,22] as well as unbiased numerical exact diagonalization (ED) analysis on finite tiles [19]. At the classical phase boundaries NAF/CAF or NAF/SP ($\phi = 0.15\pi$) and CAF/FM or SPI/FM ($\phi = 0.85\pi$), the quantum reduction of the moment diverges and long-range magnetic order is destroyed. The leads to the possibility of much discussed "spin liquid" phases reviewed in Refs. [20,23,24]. This designation is used generically for many-body ground states that do not have long-range magnetic order but rather exhibit finite range or algebraic spin correlations or show a more exotic order like valence bond solid or spin nematic state [20].

In this work, our main goal is the analysis of the overall variation of ordering temperature $T_{\mathrm{N}}(\phi, J_\perp)$ as function of control parameters in the *magnetically* ordered phases which dominate the phase diagram, using the linear spin-wave (LSW) theory. The range of ϕ values where spin-wave theory predicts the vanishing of ordered moments and becomes unreliable corresponds approximately to the narrow regions around $\phi/\pi \approx 0.15, 0.85$ where possibly a dimer spin liquid and a spin nematic phase appear, respectively. Numerous other analytical and numerical methods have been used to investigate this strongly frustrated region (Fig. 2), e.g., in Refs. [19,25–30].

The obtained J_2/J_1 or ϕ intervals of the spin liquid phase depend strongly on the method used (see Table 4 in Ref. [20]), therefore, the precise value of upper and lower boundaries of the spin liquid interval is an open question. Its absolute width as compared to the magnetic regions ($\Delta\phi/\pi \simeq 0.6$) is, however, quite small, e.g., from exact diagaonlization (ED) with scaling analysis for the square lattice model one obtains $\Delta\phi/\pi \simeq 0.075$ for the spin dimer phase interval and $\Delta\phi/\pi \simeq 0.020$ for the spin nematic interval, indicated by the gray shading in the inset of Fig. 2. It is not clear to which extent the above methods for the spin liquid regimes are able to include the effect of finite temperature and interlayer coupling. The latter may indeed further shrink the spin liquid phase interval by stabilizing magnetic order. One should note that various other additional interactions which may destabilize the spin liquid sectors [20] so that to achieve this, ground-state fine tuning of exchange parameters is necessary.

Given this situation, we restrict here to the linear spin-wave method because there it is known how a selfconsistent theory at finite temperature may be obtained empirically to calculate the ordering temperature. However, one should be aware that for ϕ inside the (not well-known) spin liquid intervals the depression of the three-dimensional (3D) ordering T_{N} is only qualitatively described by spin-wave theory and in reality may even be more rapid when approaching the center of the interval. In any case, our interest here is focused on the stable magnetic regions in the phase diagram. And there are indeed plenty of known ordered quasi-2D magnets described by the J_1-J_2 model; one extended class will be discussed in Sec. VIII. On the other hand, there is so far no compound example that realizes a spin liquid phase of the (anisotropic) triangular or square lattice, therefore, our focus on the magnetically ordered regime is empirically justified.

The quantum suppression of the ordered moment $m_{\mathbf{Q}}(\phi)$ shows considerable variation with ϕ inside the magnetic phase region and a continuous suppression to zero from both sides when approaching the quantum phase transition to the narrow spin liquid sectors. This is found from both LSW and ED [19], DMRG [30], dimer series expansion [25], and many other techniques reviewed in Ref. [20]. This naturally suggests that the actual ordering temperature $T_{\mathrm{N}}(\phi)$ of quasi-2D systems also shows considerable variation with ϕ inside the large NAF and CAF phase regions and vanishes continuously when ϕ approaches the narrow spin liquid regimes from both sides. However, there is no analysis of $T_{\mathrm{N}}(\phi)$ in the whole NAF and CAF phase sectors available. So far, mostly the $J_\perp/J_{\mathrm{c}}$ dependence of the *unfrustrated* ($\phi = 0$) AF has been investigated [9,10,31]. But, $T_{\mathrm{N}}(\phi)$ is an important practical issue because, first, many known frustrated J_1-J_2 type compounds belong to these sectors and, second, the experimental value of T_N compared to the paramagnetic Curie-Weiss temperature Θ_{CW} is usually taken as an empirical indicator of the strength of frustration in a magnet [32–34].

III. EMPIRICAL FRUSTRATION PARAMETER AND MICROSCOPIC FRUSTRATION DEGREE

For magnetic materials, in many cases two parameters are easily accessible experimentally: the paramagnetic Curie-Weiss temperature and the Néel (or Curie) temperature of the ordered phase. At high temperatures where moments become decoupled, the uniform susceptibility is described by the empirical expression

$$\chi = \frac{C}{T + \Theta_{\mathrm{CW}}}, \tag{4}$$

where C is a constant and Θ_{CW} is the Curie-Weiss temperature which is positive or negative for AF or FM materials, respectively. It is defined through the first term of the high-temperature series expansion (HTSE) of $\chi(T)$ [3] according to

$$\chi = \frac{S(S+1)}{3}\beta J_{\mathrm{c}}(1 - \beta k_{\mathrm{B}}\Theta_{\mathrm{CW}}), \tag{5}$$

$$\Theta_{\mathrm{CW}} := \frac{S(S+1)}{3k_{\mathrm{B}}}\sum_n J_{ii+n} = \frac{2S(S+1)}{3k_{\mathrm{B}}}J_{\mathbf{k}=0}, \tag{6}$$

where the susceptibility per site i is given in units of $\chi_0 = \mu_0(g\mu_{\mathrm{B}})^2/J_{\mathrm{c}}$. Explicitly, for the 3D model we have

$$k_{\mathrm{B}}\Theta_{\mathrm{CW}} = \begin{cases} \boxtimes: & J_1 + J_2 + \frac{1}{2}J_\perp, \\ \triangle: & J_1 + \frac{1}{2}J_2 + \frac{1}{2}J_\perp. \end{cases} \tag{7}$$

On the basis of a mean field (MF) approximation, Θ_{CW} is frequently associated with the AF ordering or Néel temperature T_{N} (the second experimental parameter) [35]. For the 3D (simple tetragonal or hexagonal) model, the MF values are given by

$$T_{\mathrm{N}} = \frac{2S(S+1)}{3k_{\mathrm{B}}}|J_{\mathbf{Q}}|. \tag{8}$$

This also means that the mean field Néel temperature ($S = \frac{1}{2}$) is equal to the classical ground-state energy per bond according

to $k_B T_N = |E_{cl}|/(N/2)$. Explicitly, one obtains

$$k_B T_N = \begin{cases} \boxtimes \text{ NAF}: & J_1 - J_2 + \frac{1}{2}J_\perp, \\ \boxtimes \text{ CAF}: & J_2 + \frac{1}{2}J_\perp, \\ \triangle \text{ NAF}: & J_1 - \frac{1}{2}J_2 + \frac{1}{2}J_\perp, \\ \triangle \text{ SPI}: & \frac{1}{2}J_2[1 + \frac{1}{2}(J_1/J_2)^2] + \frac{1}{2}J_\perp. \end{cases} \tag{9}$$

For the unfrustrated ($J_2 = 0$) NAF phases ($\boxtimes, \triangle$) evidently $\Theta_{CW} = T_N$, for any $J_\perp$ in mean field approximation. Naturally, the mean field expressions in Eq. (9) cease to be reasonable for $J_\perp/J_c \ll 1$ where T_N has to approach zero for the 2D lattice.

For frustrated magnets (geometrically or interaction frustrated) intuitively the temperature for long-range order should be suppressed because of the competition between exchange bonds whose exchange energy cannot be minimized simultaneously for all bonds, i. e., one would expect $T_N \ll \Theta_{CW}$ in strongly frustrated systems. Therefore, it has become customary in experimental investigations to characterize frustrated magnets by the ratio

$$f := \frac{\Theta_{CW}}{T_N}. \tag{10}$$

With T_N strongly suppressed, one would then obtain $|f| \gg 1$ with the sign given by that of Θ_{CW}. Thus, f might be regarded as a direct measure of the degree of frustration in a particular magnet [32–34].

It is not *a priori* obvious whether this widely used empirical criterion is sensible from a more microscopic point of view. An immediate problem with the definition of f is that the Curie-Weiss temperature, in particular, in frustrated magnets might be arbitrarily small as well. It can be even zero or negative, also for materials with AF order, due to competing interactions with opposite sign. In the simple mean field approach applicable only for reasonably large $J_\perp/J_c$ the corresponding f is shown in Fig. 3. Moderately enhanced values $|f| > 1$ are only found around the NAF/CAF ($\square$) or NAF/SPI ($\triangle$) boundaries ($\phi/\pi = 0.15$). On approaching the FM region from both sides $|f|$ does not show an enhancement due to the smallness of $|\Theta_{CW}|$. In

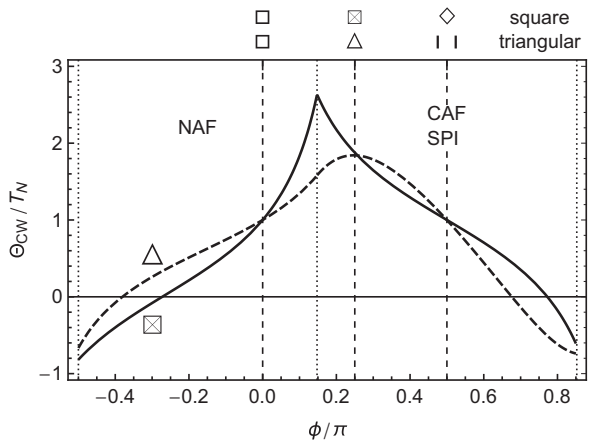

FIG. 3. Frustration ratio $f = \Theta_{CW}/T_N$ using mean field T_N for triangular (dashed line) and square (solid line) lattice model with $J_\perp/J_c = 0.2$.

fact, for $\phi < 0$ ($J_2 < 0$) this should not be expected because in this case the model is unfrustrated (Fig. 2).

On the other hand, microscopically frustration is understood as the impossibility to minimize the ground-state energy simultaneously for all exchange bonds. Therefore, it appears natural to compare the ground-state energy of the minimal building blocks of the frustrated lattice to the total ground-state energy of the unfrustrated components. For example, this can be achieved by defining the degree of frustration in the triangular lattice according to [3]

$$\kappa_\triangle := 1 - \frac{E_\triangle}{E_t + E_d} \tag{11}$$

for the frustrated triangle where $E_\triangle$ is its ground-state energy and $E_{t,d}$ are those of its constituents, i. e., decoupled trimer and dimer. Explicitly [3],

$$E_\triangle(\phi) = \min\left(-\tfrac{3}{4}J_2, -J_1 + \tfrac{1}{4}J_2, \tfrac{1}{2}J_1 + \tfrac{1}{4}J_2\right) \tag{12}$$

from which we also obtain $E_t := E_\triangle(J_2 = 0)$ and $E_d := E_\triangle(J_1 = 0)$. A similar definition can be made for $\kappa_\boxtimes$ of the J_1-J_2 square lattice where the constituents are the unfrustrated square and the two diagonal dimer bonds. It turns out that $\kappa_\boxtimes(\phi) \equiv \kappa_\triangle(\phi) =: \kappa(\phi)$. This function indeed vanishes in the unfrustrated regime $J_2 < 0$ or $-\pi \leqslant \phi \leqslant 0$. For $J_2 > 0$, the triangular lattice becomes frustrated, and κ strictly monotonously increases until its maximum value $\kappa(\pi/4) = 4/7 \approx 0.57$ which is the 2D isotropic point in the triangular phase diagram. Then, κ decreases to $\kappa(\pi/2) = 0$ which is the point where the triangular lattice decouples into independent, unfrustrated AF chains. In the square lattice this case corresponds to two decoupled unfrustrated pure Néel sublattices. For ferromagnetic $J_1 < 0$ or $\phi > \pi/2$, κ increases again to reach a maximum at the border between the spiral and FM phases. Therefore, κ peaks at or close to the strongly frustrated regions of the classical phase boundaries (Fig. 2) where magnetic order disappears. The large frustration is not only reflected in this ground-state measure but also leads to signatures in the excited state spectrum. Full diagonalization of small clusters [20] shows that for ϕ values where $\kappa(\phi)$ approaches maximum the excited states are closely spaced and have large degeneracies. In the thermodynamic limit, this signifies the strong suppression and breakdown of the ordered moment.

The qualitative behavior of $\kappa(\phi)$ therefore faithfully maps the degree of frustration as function of frustration control parameter ϕ. It is now a legitimate question to ask whether the quasi-2D Néel temperature $T_N(\phi)$ and empirical frustration ratio $|f(\phi)|$ show a depression or enhancement, respectively, in the same region where $\kappa(\phi)$ is large. For the simple mean field model, the results are shown in Fig. 3. In fact, at the $\phi/\pi \simeq 0.15$ phase boundary the peak in the frustration degree $\kappa(\phi)$ (Fig. 2) coincides with the enhancement of f. On the $\phi/\pi \simeq 0.85$ classical boundary to the FM where Θ_{CW} has to change sign, however, no such coincidence is possible. It is important to investigate this further for the really interesting quasi-2D magnets. This requires a more advanced self-consistent RPA spin-wave approach to calculate $T_N(\phi)$.

IV. LSW AND RPA CALCULATION OF THE QUASI-2D NÉEL TEMPERATURE

A calculation of T_N implies a theory of spin excitations at finite temperatures. This is a difficult problem from a fundamental point of view. In the linear spin-wave (LSW) approximation and its various generalizations, the spin excitations are described by bosons whose density increases with temperature, necessitating the inclusion of interaction effects [36] beyond LSW. An effective empirical way to circumvent this difficult-to-treat many-body problem is provided by the Tyablikov method [11,14] which assumes that the spin-wave energy scale is reduced in accordance with the decreasing ordered moment, instead of staying fixed as in LSW. It corresponds to an effective RPA approximation of the spin-wave propagator [9,11,13]. As noted in Ref. [14], the Tyablikov approach is "satisfactory from the practical but not from the theoretical point of view." Since we take the former view and want to apply it to a general and practical understanding of frustration dependence of T_N, we use the Tyablikov approach, generalized to finite fields in this work. This is supported by a comparison to unbiased numerical MC simulations for the NN 2D Heisenberg model [10] without field which prove that the numerical results show excellent agreement with RPA approximation throughout the whole range of $J_\perp/J_1$ ratios.

For the sake of a self-contained presentation we first recapitulate the LSW results of the J_1-J_2 model in an external field in a form that is applicable to square as well as triangular lattice models. It is obtained from Eq. (1) by adding the Zeeman term leading to the full Hamiltonian $\mathscr{H} = \mathscr{H}_{ex} - \mathbf{h}\cdot\sum_i \mathbf{S}_i$ with the definition $\mathbf{h} = g\mu_B\mu_0\mathbf{H}$. In the LSW, a Holstein-Primakoff (HP) transformation from local spin variables S_i^α ($\alpha = x,y,z$) to bosonic variables $a_i, a_i^\dagger$ at site i is carried out using $S_i^+ \to \sqrt{S/2}a_i$, $S_i^- \to \sqrt{S/2}a_i^\dagger$, and $S_i^z \to S - a_i^\dagger a_i$. Then, performing the Fourier transform

$$a_i = \frac{1}{\sqrt{N}}\sum_{\mathbf{k}} a_{\mathbf{k}}^\dagger e^{-i\mathbf{k}\cdot\mathbf{R}_i}, \tag{13}$$

the total Hamiltonian $\mathscr{H}$ may be written as a bilinear (harmonic) form in $\hat{a}_{\mathbf{k}}^\dagger = (a_{\mathbf{k}}^\dagger, a_{-\mathbf{k}})$ which may be diagonalized [Eq. (15)] by the Bogoliubov transformation $\alpha_{\mathbf{k}} = u_{\mathbf{k}}a_{\mathbf{k}} + v_{\mathbf{k}}a_{-\mathbf{k}}^\dagger$ to the magnon creation and annihilation operators $\alpha_{\mathbf{k}}, \alpha_{\mathbf{k}}^\dagger$ of spin-wave modes given in Eq. (16). The transformation coefficients are obtained as

$$\left\{\begin{matrix} u_{\mathbf{k}}^2 \\ v_{\mathbf{k}}^2 \end{matrix}\right\} = \frac{1}{2}\left[\frac{A_{\mathbf{k}} - B_{\mathbf{k}}\cos^2\Theta_{cl}}{E_{\mathbf{k}}} \pm 1\right] \tag{14}$$

with the sign convention $u_{\mathbf{k}} = \text{sign}\, B_{\mathbf{k}}|u_{\mathbf{k}}|$, $v_{\mathbf{k}} = |v_{\mathbf{k}}|$, and $SE_{\mathbf{k}}$ denoting the symmetric part of magnon energies given below. In the spirit of a $(1/S)$ expansion, the classical value Θ_{cl} of the moment canting angle ($\Theta_{cl} = \pi/2$ for zero field) is used in Eq. (14) as given by $\cos\Theta_{cl} = h/h_s$. Here $h_s = 2SA_0 = 2S(J_0 - J_{\mathbf{Q}})$ is the saturation field where the moments are aligned with the field ($\Theta_{cl} = 0$). This means $h_s/2S = 4J_1$ for NAF and $h_s/2S = 2(J_1 + 2J_2)$ for CAF. The final result of the HP transformation is then the free magnon Hamiltonian

$$\begin{aligned} \mathscr{H} &= E_{cl} + E_{zp} + S\sum_{\mathbf{k}} E_{\mathbf{k}}^{sw}\alpha_{\mathbf{k}}^\dagger\alpha_{\mathbf{k}}, \\ E_{cl} &= NS^2(J_{\mathbf{Q}} - A_0\cos^2\Theta_{cl}), \\ E_{zp} &= NSJ_{\mathbf{Q}} + \frac{S}{2}\sum_{\mathbf{k}} E_{\mathbf{k}}. \end{aligned} \tag{15}$$

Here, E_{cl} is the (negative) classical ground-state energy, the second term E_{zp} is the (negative) energy of zero-point fluctuations of magnon modes, and the last term describes the free Hamiltonian of excited magnons. The total ground-state energy is $E_{gs} = E_{cl} + E_{zp}$. The zero-point contribution is of relative order $1/S$ as compared to the classical part. The bare spin-wave or magnon energy $\omega_{\mathbf{k}} = SE_{\mathbf{k}}^{sw}$ is obtained from the Bogoliubov transformation as

$$\begin{aligned} E_{\mathbf{k}}^{sw} &= E_{\mathbf{k}} + E_{\mathbf{k}}^a, \\ E_{\mathbf{k}} &= \sqrt{[A_{\mathbf{k}} - B_{\mathbf{k}}][A_{\mathbf{k}} + B_{\mathbf{k}}(1 - 2\cos^2\Theta_{cl})]}, \\ E_{\mathbf{k}}^a &= C_{\mathbf{k}}\cos\Theta_{cl}, \end{aligned} \tag{16}$$

where intrasublattice and intersublattice interactions $A_{\mathbf{k}}$ and $B_{\mathbf{k}}$ as well as the interaction term $C_{\mathbf{k}} = -C_{-\mathbf{k}}$ which are symmetric and antisymmetric in $\mathbf{k}$, respectively, are given by

$$\begin{aligned} A_{\mathbf{k}} &= J_{\mathbf{k}} + \tfrac{1}{2}(J_{\mathbf{k}+\mathbf{Q}} + J_{\mathbf{k}-\mathbf{Q}}) - 2J_{\mathbf{Q}}, \\ B_{\mathbf{k}} &= J_{\mathbf{k}} - \tfrac{1}{2}(J_{\mathbf{k}+\mathbf{Q}} + J_{\mathbf{k}-\mathbf{Q}}), \\ C_{\mathbf{k}} &= J_{\mathbf{k}+\mathbf{Q}} - J_{\mathbf{k}-\mathbf{Q}}. \end{aligned} \tag{17}$$

Note that in general $E_{\mathbf{k}}^{sw}$ is *not* symmetric under $\mathbf{k} \to -\mathbf{k}$ because $E_{-\mathbf{k}}^{sw} = E_{\mathbf{k}} - E_{\mathbf{k}}^a$ and therefore $E_{\mathbf{k}}^{sw} - E_{-\mathbf{k}}^{sw} = 2E_{\mathbf{k}}^a \neq 0$. The asymmetric term is only relevant when $2\mathbf{Q}$ is *not* a reciprocal lattice vector, i.e., in the present context only in the spiral phase of the triangular lattice for $\mathbf{H} \neq 0$. In zero field where $E_{\mathbf{k}}^a = 0$, $\Theta_{cl} = \pi/2$, Eq. (16) reduces to

$$E_{\mathbf{k}}^{sw} = E_{\mathbf{k}} = \sqrt{A_{\mathbf{k}}^2 - B_{\mathbf{k}}^2}. \tag{18}$$

Equations (16) and (18) are the basic quantities needed to calculate the Néel temperature and H-T phase diagram of the frustrated models within the Tyablikov RPA approach. This amounts to a stark simplification of the real interacting magnon problem. In fact, due to the intrinsic interaction of magnons originating from higher-order terms of the HP transformation already at zero temperature the magnon spectral function is renormalized [38]. In the strongly frustrated spin (dimer) liquid regime the spectrum may change qualitatively, consisting of a singlet bound state with finite gap, split off from the two-magnon (triplon) continuum [39]. The gap closes at the quantum transition (as function of ϕ) to the neighboring antiferromagnetic phases. These approaches are, however, difficult to generalize to finite temperature and finite interlayer coupling. As pointed out previously [14], the empirical Tyablikov RPA method radically simplifies the problem by neglecting the change of spectral shape in the spin excitations due to multimagnon interactions. It circumvents the complicated many-body processes by assuming that one still has a free magnon spectrum at higher temperature but with an overall dispersive width proportional to the T-dependent order parameter. This enforces a self-consistency condition from

which $T_N(\phi, J_\perp)$ may be derived. While this seems acceptable in the magnetically ordered regimes, it can only provide a qualitative interpolation across the narrow spin liquid regimes of ϕ. In reality, $T_N(\phi, J_\perp)$ has to be expected to be suppressed even more rapidly than predicted by the spin-wave theory in these narrow ϕ intervals.

Rather than deriving the dynamical Green's function as in Ref. [9] for the present purpose it is sufficient to calculate the self-consistent static moment directly. The condition that it vanishes will then determine the Néel temperature. The total moment at a site i is given by the thermal expectation value (with respect to $\mathscr{H}$) $\langle S_i^{z'}\rangle$ in the *local* coordinate system the components of which we denote with a prime. In this coordinate system, the z' axis at a given site site i is aligned with the moment direction at that site. The latter is canted out of the plane given by the ordering vector $\mathbf{Q}$ due to the effect of the magnetic field which is directed along the global z axis. The relation between moments in the local and global coordinate systems is given in Appendix A.

In a finite magnetic field, we have to distinguish three types of moments: the total moment $\langle S\rangle$, homogeneous moment m_0, and ordered moment $m_{\mathbf{Q}}$. While we consider all phases for zero field, in finite field we will restrict to the commensurate CAF and NAF structures. For these coplanar cases the canted moments may be considered to lie in the xz plane. Then, we have the definitions

$$\begin{aligned} \langle S\rangle &= \frac{1}{N}\sum_i \langle S_i^{z'}\rangle, \\ m_0 &= \frac{1}{N}\sum_i \langle S_i^{z}\rangle, \\ m_{\mathbf{Q}} &= \frac{1}{N}\sum_i \mathrm{e}^{\mathrm{i}\mathbf{Q}\cdot\mathbf{R}_i}\langle S_i^{x}\rangle. \end{aligned} \tag{19}$$

(All moments are expressed in units of the Bohr magneton μ_B.) Using the transformation in Appendix A, one can verify that $m_0 = \langle S\rangle \cos\Theta_{cl}$, $m_{\mathbf{Q}} = \langle S\rangle \sin\Theta_{cl}$, and then $\langle S\rangle^2 = m_0^2 + m_{\mathbf{Q}}^2$.

For $S = \frac{1}{2}$ we can write $S_i^{z'} = \frac{1}{2} - S_i^{-'}S_i^{+'}$. According to the linearized HP approximation for $S = \frac{1}{2}$ we then have $\langle S\rangle = (\frac{1}{2}) - 2S\langle a_i^\dagger a_i\rangle$. In the moment reduction part of the right-hand side we now replace $S \to \langle S\rangle$. Physically, this means that the reduction of the moment from $\frac{1}{2}$ due to the number of thermally excited Holstein-Primakoff bosons $\psi := \langle a_i^\dagger a_i\rangle$ per site is rescaled by the already reduced moment $\langle S\rangle$. This substitution leads then to a self-consistency condition for the moment according to

$$\langle S\rangle = \frac{1/2}{1+2\psi}, \quad \psi = \langle a_i^\dagger a_i\rangle = \int_{BZ}\frac{d^3k}{V_{BZ}}\langle a_{\mathbf{k}}^\dagger a_{\mathbf{k}}\rangle, \tag{20}$$

where $\langle \dots \rangle$ denotes the thermal average with respect to the magnon Hamiltonian of Eq. (15). Unless otherwise noted, here and in the following we use continuum notation in reciprocal space, and integrations are done over the chemical Brillouin zone with volume V_{BZ}.

If ψ is small (at low temperature) then $\langle S\rangle \simeq 1/2 - \psi$ which recovers the LSW expression for the moment. The result of this simple physical consideration in Eq. (20) is equivalent to the RPA result [9] which also determines the temperature dependence of correlation functions in addition to the total moment. Here, we only want to find the Néel temperature from the condition $m_{\mathbf{Q}} = 0$. To this end, one has to calculate $\psi = \psi(T,H)$ using the Bogoliubov transformation to magnon operators $\alpha_{\mathbf{k}}, \alpha_{\mathbf{k}}^\dagger$ leading to

$$\psi(T,H) = \int_{BZ}\frac{d^3k}{V_{BZ}}\left[v_{\mathbf{k}}^2 + \left(1+v_{\mathbf{k}}^2\right)\langle\alpha_{\mathbf{k}}^\dagger\alpha_{\mathbf{k}}\rangle + v_{\mathbf{k}}^2\langle\alpha_{-\mathbf{k}}^\dagger\alpha_{-\mathbf{k}}\rangle\right]. \tag{21}$$

Using Eq. (14) this may be evaluated to give the denominator in Eq. (20) and we finally obtain the self-consistency equation for the temperature- and field-dependent total moment as

$$\langle S\rangle = \frac{1}{2}\left(\int_{BZ}\frac{d^3k}{V_{BZ}}\frac{A_{\mathbf{k}} - B_{\mathbf{k}}\cos^2\Theta_{cl}}{E_{\mathbf{k}}}\coth\frac{\beta\langle S\rangle E_{\mathbf{k}}^{sw}}{2}\right)^{-1}, \tag{22}$$

where $\beta = 1/(k_B T)$. It is important to note that here $\Omega_{\mathbf{k}} = \langle S\rangle E_{\mathbf{k}}^{sw}$ is the modified magnon energy scaled by the temperature-dependent prefactor $\langle S\rangle$ instead of the constant $S = \frac{1}{2}$ as in LSW approximation.

The Néel temperature $T_N = 1/(k_B\beta_N)$ itself is defined as the temperature where the ordered moment vanishes. For small magnetic fields with $h/h_s \ll \beta_N(h=0)J_c/4$, we can identify the ordered moment $m_{\mathbf{Q}}$ with the total moment $\langle S\rangle$. Expanding Eq. (22) for $\langle S\rangle \ll 1$ to leading order, we obtain a closed expression

$$\beta_N(h) = 4\int_{BZ}\frac{d^3k}{V_{BZ}}\frac{A_{\mathbf{k}} - B_{\mathbf{k}}\cos^2\Theta_{cl}}{E_{\mathbf{k}}^2 - E_{\mathbf{k}}^{a2}}. \tag{23}$$

Below T_N the T dependence of the ordered moment $\langle S\rangle$ is obtained by an iterative solution of Eq. (22). To improve numerical convergence, it is preferable to separate out the singular term in the integrand by defining $g(x) = \coth(x) - 1/x$ leading to a numerically more suitable form of the self-consistency equation:

$$\begin{aligned} \langle S\rangle = \frac{1}{2}&\left(1 - \frac{\beta_N}{\beta}\right) \\ &\times\left[\int_{BZ}\frac{d^3k}{V_{BZ}}\frac{A_{\mathbf{k}} - B_{\mathbf{k}}\cos^2\Theta_{cl}}{E_{\mathbf{k}}}g\left(\frac{\beta\langle S\rangle E_{\mathbf{k}}}{2}\right)\right]^{-1}, \end{aligned} \tag{24}$$

where the integral in brackets is now a well-behaved function near $T = T_N$. Its expansion for small $\langle S\rangle$ leads to an approximate expression close to T_N:

$$\begin{aligned} \langle S\rangle \approx \sqrt{\frac{1-\beta_N/\beta}{\beta_N I_0}}&\left[1 + \frac{1}{2}\left(1 - \frac{\beta_N}{\beta}\right)\frac{\beta_N I_1}{I_0^2}\right. \\ &\left. - \frac{1}{2}\left(1 - \frac{\beta_N}{\beta}\right)^2\frac{\beta_N^2}{I_0^4}\left(I_0 I_2 - \frac{7}{4}I_1^2\right)\right], \end{aligned} \tag{25}$$

where the expansion integrals I_{0-2} are given in Appendix B. A comparison of numerical solution and analytical approximation for a CAF and NAF case is shown in Fig. 4. The global behavior of the zero-field total moment $\langle S\rangle(T,\phi)$ as function of temperature and frustration control parameter is depicted in the 3D plot of Fig. 5 for both lattices.

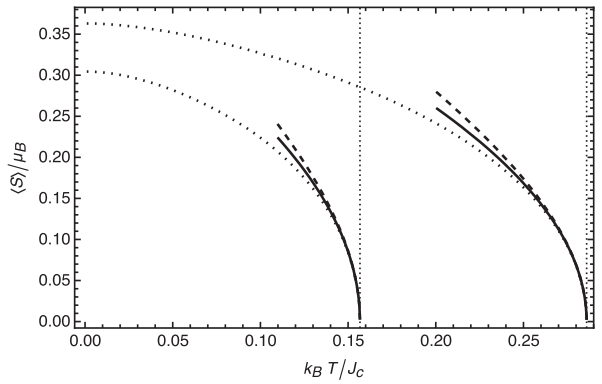

FIG. 4. Ordered moment temperature dependence of square lattice for two frustration parameters $\phi \approx 0$ (pure NAF, lower set of curves) and $\phi \approx 0.6\pi$ (CAF with FM J_1). The numerical solutions of Eq. (24) (dotted line) are compared with analytical solution of Eq. (25) comprising first-order (full line) and second-order (dashed line) terms. The vertical dotted lines indicate the respective T_N.

The self-consistency equation (22) may also be used to calculate the field dependence of the Néel temperature. It is defined by the condition that the order parameter vanishes, i.e., $m_{\mathbf{Q}} = 0$. Then, the total moment is equal to the magnetization per site $\langle S\rangle = m_0$. For simplicity, we use the classical value $m_0 = (\frac{1}{2})\cos\Theta_{\rm cl}$. Furthermore, m_0 may be taken as T independent as long as $k_{\rm B}T_{\rm N} \ll J_{\rm c}$.

Replacing $\langle S\rangle \to m_0$ in Eq. (22) gives an implicit equation for $T_{\rm N} = T_{\rm N}(h)$. It may be presented in a form more convenient for numerical solution as

$$T_{\rm N} = \tilde{T}_{\rm N}\left[1 - 2m_0 \int_{\rm BZ} \frac{d^3k}{V_{\rm BZ}} \frac{A_{\mathbf{k}} - B_{\mathbf{k}}\cos^2\Theta_{\rm cl}}{E_{\mathbf{k}}}\, g\left(\frac{m_0 E_{\mathbf{k}}}{2k_{\rm B}T_{\rm N}}\right)\right], \tag{26}$$

where $\tilde{T}_{\rm N} = 1/(k_{\rm B}\beta_{\rm N})$ now denotes the small-field expression from Eq. (23). For $h \ll h_{\rm s}$ when $m_0 \to 0$ we indeed recover Eq. (23).

For $h = 0$ and for general h in the nonspiral (NAF, CAF) phases the asymmetric term $\sim E^{a2}_{\mathbf{k}}$ in the spin-wave dispersion vanishes and $E^{\rm sw}_{\mathbf{k}} = E_{\mathbf{k}}$. The zero-field limit $T^0_{\rm N} := T_{\rm N}(h \to 0)$ is then given by [9]

$$T^0_{\rm N} = \left(4k_{\rm B}\int_{\rm BZ} \frac{d^3k}{V_{\rm BZ}} \frac{A_{\mathbf{k}}}{E^2_{\mathbf{k}}}\right)^{-1}. \tag{27}$$

This is an explicit expression for $T^0_{\rm N}$ which does not contain $T^0_{\rm N}$ on the right-hand side any more. It properly reproduces the 2D limit $T^0_{\rm N} \to 0$ when the k_z dispersion of magnons vanishes and the integral in Eq. (27) diverges logarithmically (see Sec. VI). The above equations contain all information on the frustration effect encoded in the spin-wave expressions $A_{\mathbf{k}}$, $B_{\mathbf{k}}$, and $E_{\mathbf{k}}$ of Eqs. (16) and (17).

V. NUMERICAL RESULTS FOR THE ZERO-FIELD NÉEL TEMPERATURE

In this section we discuss the systematic variation of $T_{\rm N}(\phi)$ with frustration control parameter $\phi = \tan^{-1}(J_2/J_1)$ as obtained from the numerical calculations based on Eq. (27) for square as well as triangular models.

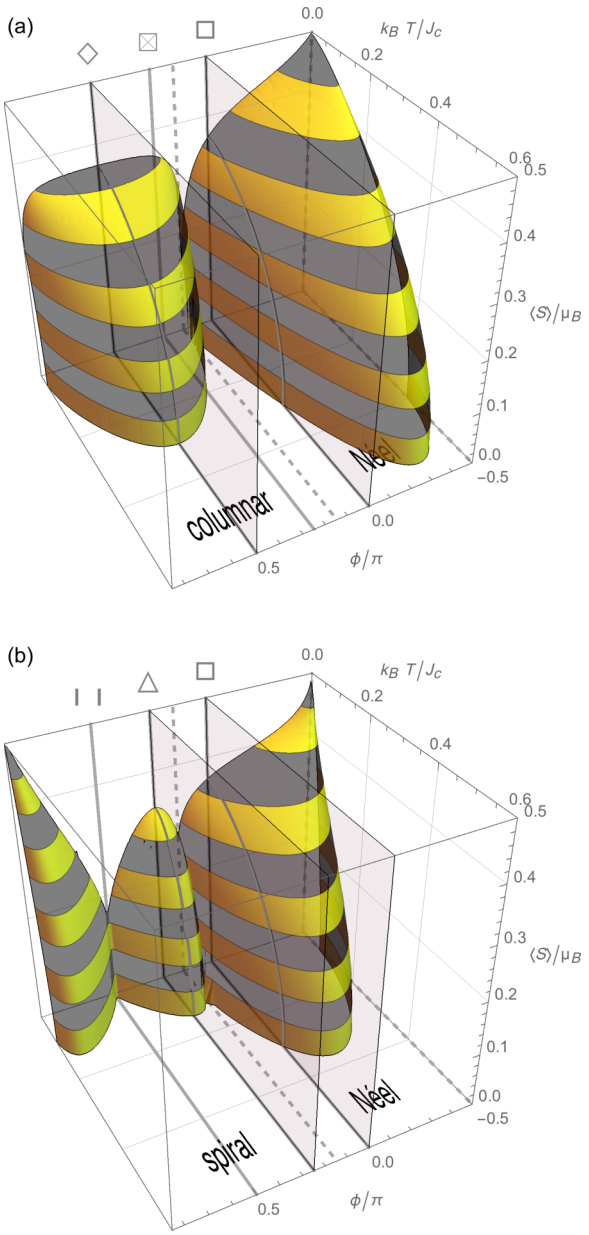

FIG. 5. Zero-field ordered moment $\langle S\rangle$ (ordinate) in ϕ-T plane for the square lattice (a) and triangular lattice (b), using $J_\perp/J_{\rm c} = 0.01$. The $\langle S\rangle = 0$ cut (basal plane) gives the $T_{\rm N}(\phi)$ curves in Figs. 7(a) and 8(a) for square and triangular cases. The $T = 0$ cut (backside plane) likewise gives the ground-state ordered moment $m_{\mathbf{Q}}(\phi)$ [19,22,37]. Both curves are topologically equivalent and reach zero for ϕ values with strong frustration ($\phi/\pi \simeq 0.15, 0.85$). In (b) the additional zero at $\phi/\pi = 0.5$ is not due to frustration but corresponds to unfrustrated quasi-1D AF chain case.

A. Square-lattice model

Figure 6(a) displays the dependence of $T_{\rm N}$ obtained from Eq. (27) on the interplane coupling $J_\perp$ for selected values of ϕ. The approximately logarithmic variation with $J_\perp/J_{\rm c}$ known from the pure Néel case is observed to hold also in the frustrated case (see Sec. VI). In this case ($J_2 = 0$, $J_{\rm c} = J_1$) there are MC simulation results [10] for T_N which can be compared to the results of the present theory [Fig. 6(b)]. They

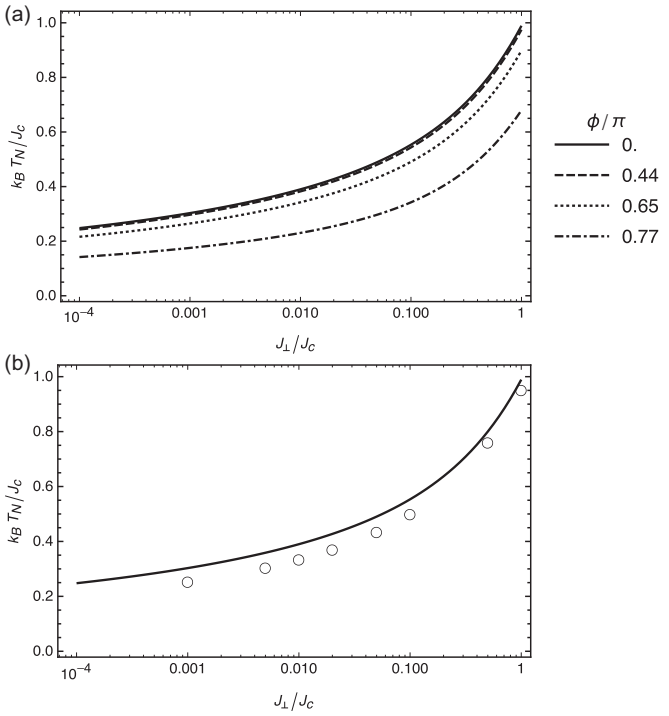

FIG. 6. (a) T_N dependence on $J_\perp/J_c$ for various frustration control parameters ϕ in the square-lattice model in the NAF and CAF phases. (b) T_N for the unfrustrated ($\phi = 0$ or $J_2 = 0$, $J_c = J_1$) pure Néel case. Full line same as in (a). The open circles are from MC simulations in Ref. [10]. Note the additional ordinate scale factor $S(S+1) = \frac{3}{4}$ employed in this reference.

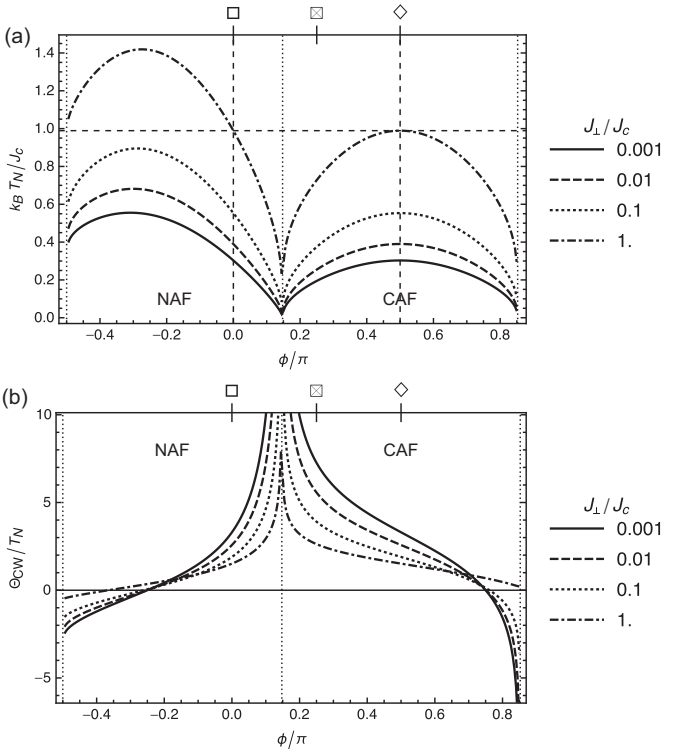

FIG. 7. Quasi-2D Néel temperature T_N (a) and empirical frustration ratio $f = \Theta_{CW}/T_N$ (b) for the square lattice J_1-J_2 as function of frustration control parameter ϕ for different interlayer coupling strengths $J_\perp/J_c = 10^{-3} \ldots 1$.

show a good agreement within only a few percent deviation in the whole range of $J_\perp/J_c$ plotted [40].

In the complementary Fig. 7(a) we show the Néel temperature $T_N(\phi)$ at different strengths of the interplane coupling $J_\perp/J_c = 10^{-3} \ldots 1$. T_N vanishes at the borders of the columnar phase (see Appendix C). In the isotropic 3D cases with $J_1 = J_\perp = J_c$, $J_2 = 0$, and $J_1 = 0$, $J_2 = J_\perp = J_c$, the result $k_B T_N/J_c \approx 0.989$ is obtained. Note that the corresponding MF result [Eq. (9)] would be $k_B T_N/J_c = \frac{3}{2}$. The symmetric ϕ dependence in the CAF phase is due to a mirror symmetry of the Hamiltonian at $J_1 = 0$ ($\phi = \pm\pi/2$): the square lattice is bipartite and the Hamiltonian remains invariant upon a sign change of all spins on one sublattice while simultaneously replacing $J_1 \to -J_1$. This transforms the Néel antiferromagnet to a ferromagnet (not shown) and the CAF phase with $(\pi,0)$ ordering into $(0,\pi)$ ordering.

For the $S = \frac{1}{2}$ frustrated square lattice, the Curie-Weiss temperature is given by $\Theta_{CW} = (J_1 + J_2 + J_\perp/2)/k_B$ [Eq. (7)]. Figure 7(b) displays the corresponding parameter $f = \Theta_{CW}/T_N$ as a function of ϕ for different interlayer coupling strengths $J_\perp/J_c = 10^{-3} \ldots 1$. The overall ϕ dependence is in good agreement with the approximate analytical evaluation of Eq. (27) in Sec. VI.

It is instructive to compare $f(\phi)$ with the behavior of the microscopic frustration degree $\kappa(\phi)$ shown in Fig. 2 [Eq. (11)]. In the Néel phase, we indeed obtain a correspondence between κ and f: where $\kappa \equiv 0$, in the whole unfrustrated NAF phase as well as at $\phi = \pi/2$, we correspondingly obtain $|f| = \mathcal{O}(1)$. This is true even for the quasi-2D case and $|f|$ appears to increase only logarithmically with decreasing $J_\perp/J_c$. (In the regions $\phi < -\pi/4$, f turns negative because $\Theta_{CW} < 0$ due to a ferromagnetic $J_2 < -J_1 < 0$.)

A finite positive J_2 turns on frustration with $\kappa > 0$. In the Néel phase, this is reflected by a corresponding increase in f which eventually diverges at the NAF/CAF border. Here, $J_2 = J_1/2$ and $\kappa = 4/11 \approx 0.36$.

The analogy between κ and f partially fails in the CAF phase: κ does not show any special feature at the NAF/CAF border but instead increases strictly monotonously to its maximum value $\kappa = 4/7 \approx 0.57$ at $J_2 = J_1$ ($\phi = \pi/4$). It then decreases and vanishes again at the special point $\phi = \pi/2$ where $J_1 = 0$ with decoupled sublattices that correspond to the pure Néel case of $\phi = 0$. For $\phi > \pi/2$, J_1 turns ferromagnetic, leading to an increase in κ until the FM border of the CAF phase where $J_2 = -J_1/2$ and $\kappa = \frac{4}{7}$ again. Different to the behavior of κ, $|f|$ is diverging at both the border to the NAF and the border to the FM phase. With increasing ϕ, f decreases strictly monotonously, crossing $f = 0$ at $\phi > 3\pi/4$ due to the sign change of Θ_{CW}.

B. Anisotropic triangular-lattice model

In Fig. 8(a) we show the parameter dependence of the Néel temperature for the $S = \frac{1}{2}$ anisotropic triangular lattice. Different curves correspond to different interplane couplings $J_\perp/J_c = 10^{-3} \ldots 1$. In the Néel phase for $-\pi/2 \leqslant \phi \leqslant \tan^{-1}(\frac{1}{2}) \approx 0.15\pi$, the qualitative behavior is similar to the

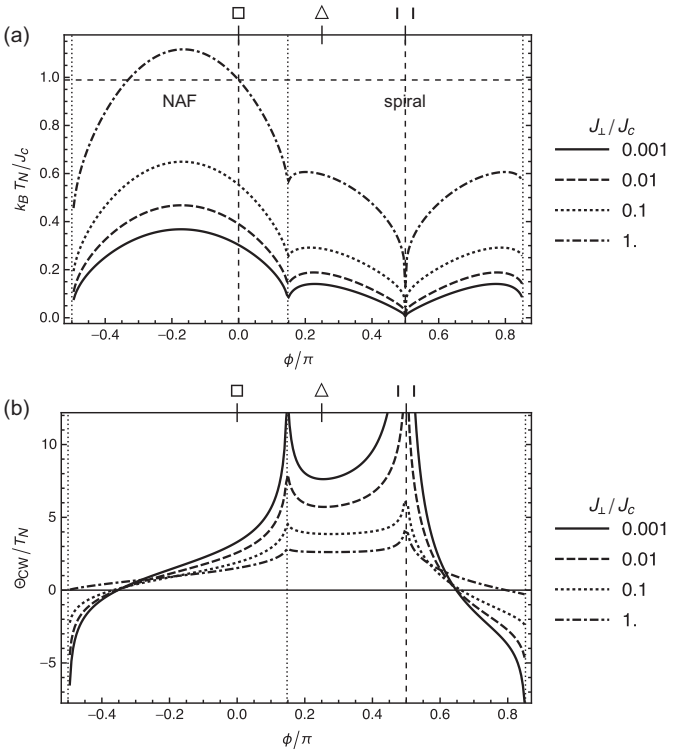

FIG. 8. Quasi-2D Néel temperature T_N (a) and empirical frustration ratio $f = \Theta_{CW}/T_N$ (b) for the triangular lattice J_1-J_2 as function of frustration control parameter ϕ for different interlayer coupling strengths $J_\perp/J_c = 10^{-3} \ldots 1$.

square-lattice case: T_N increases from zero at $\phi = -\pi/2$ ($J_1 = 0$, $J_2 = -J_c < 0$) to a maximum in the middle of the NAF phase and decreases to a cusplike minimum at $J_2/J_1 = \frac{1}{2}$ ($\phi \approx 0.15\pi$), the border with the spiral phase in the LSW approximation. The Néel temperature decreases again towards $T_N = 0$ at $\phi = \pi/2$ ($J_1 = 0$, $J_2 = J_c > 0$). At this particular point in the phase diagram the triangular lattice turns into an unfrustrated set of independent one-dimensional AF J_2 chains coupled by $J_\perp$, i.e., a strictly 2D magnet. The ordering temperature thus vanishes *not* due to frustration but can be understood as a consequence of the Mermin-Wagner theorem. The mirror symmetry in the spiral phase around $\phi = \pi/2$ is due to the same mirror symmetry present in the Hamiltonian for the square lattice, regarding the anisotropic triangular lattice as a depleted J_1-J_2 square lattice where one set of diagonal J_2 bonds is missing.

It is again useful to compare $f(\phi)$ with the microscopic degree of frustration $\kappa(\phi)$ (Fig. 2). Now, the Curie-Weiss temperature is given by $\Theta_{CW} = (J_1 + J_2/2 + J_\perp/2)/k_B$ [Eq. (7)]. In the Néel phase with ferromagnetic $J_2 < 0$ ($\kappa = 0$, unfrustrated for $-\pi/2 \leqslant \phi \leqslant 0$), we generally obtain $|f| = \mathcal{O}(1)$ for $J_\perp = J_c$ and its maximum value increases only logarithmically with decreasing interlayer coupling $0 < J_\perp/J_c < 1$. This is similar to the square-lattice case. However, except for an isotropic interlayer coupling $J_\perp = J_c$ where $\Theta_{CW} = 0$, $|f|$ diverges at the NAF/FM border ($J_1 = 0$ or $\phi/\pi = -0.5$). Like for antiferromagnetic J_2 as discussed in the preceding paragraph, this divergence is caused by a vanishing T_N at the border which is also due to the formation of a strictly two-dimensional system consisting of ferromagnetic J_2 chains coupled with $J_\perp$.

A peak appears at the NAF/SPI border ($\phi/\pi = 0.15$) which is, as in the square-lattice case, not reflected by any special feature in $\kappa(\phi)$. At $J_1 = 0$ or $\phi/\pi = 0.5$ again a divergence due to vanishing T_N appears, this time at the antiferromagnetic $J_2 > 0$ side of the phase diagram. We have $\kappa(\pi/2) = 0$ here because, at this point, the model is unfrustrated and the divergence of f is exclusively due to the previously discussed lowering of dimensionality. Another peak in $|f|$ for small $J_\perp$ is present at the SPI/FM boundary ($J_2 = -J_1/2$, $\phi/\pi \approx 0.85$).

Altogether only the two peaks in $|f(\phi)|$ at the NAF/SPI and SPI/FM boundaries can be associated with the regions of high frustration [large $\kappa(\phi)$ in Fig. 2]. The divergences in $|f|$ at $\phi = \pm\pi/2$ in contrast are unrelated to frustration effects but are due to dimensional reduction only. This does not appear in the square lattice (Fig. 7) because of the additional J_2 bond.

VI. ANALYTICAL APPROXIMATIONS FOR THE NÉEL TEMPERATURE

It is useful to complement the numerical determination of zero field $T_N(\phi, J_\perp)$ with approximate analytical results to gain a better understanding of the frustration influence. They are derived by expanding the integrand in Eq. (27) for small $\mathbf{k}$ vectors where $E_\mathbf{k}$ tends to zero; this region dominates the value of the integral. For NAF there are two equivalent dispersion minima $\mathbf{k} \approx (0,0),(\pi,\pi)$ for NAF phase and four equivalent minima positions $\mathbf{k} \approx (0,0),(0,\pi),(\pi,0),(\pi,\pi)$ for CAF phase. The expansion has to be done separately for each magnetic structure and the cutoff wave vectors in both cases have to be chosen such that the symmetry $T_N(J_1 = 0) = T_N(J_2 = 0)$ is preserved. We will restrict ourselves in this section to the NAF and CAF phases of the square lattice only.

A. NAF structure ($2J_2 < J_1$)

Here, the expansion of $E_\mathbf{k}$ and $A_\mathbf{k}$ to lowest order leads to

$$k_B T_N = \left[\frac{4}{\pi^3} \int_0^\pi \int_0^{k_\parallel^c} \frac{d^2 k_\parallel}{\tilde{J} k_\parallel^2 + J_\perp k_z^2} \right]^{-1}, \tag{28}$$

where we defined the effective exchange $\tilde{J} := J_1 - 2J_2 > 0$ for the frustrated NAF and $\varepsilon^2 := J_\perp/\tilde{J}$ as the parameter that measures the relative strength of interlayer coupling. The integral diverges, i.e., $T_N \to 0$ in the purely 2D case ($J_\perp = 0$) and also when approaching the classical NAF/CAF phase boundary at $\tilde{J} = 0$ ($2J_2 = J_1$) where the ordered moment vanishes due to strong frustration effect. The value of T_N depends weakly on the cutoff which we choose as $k_\parallel^c = \pi$ corresponding to a Debye approximation for the spin-wave spectrum. The evaluation of Eq. (28) leads to

$$k_B T_N = (J_1 - 2J_2) \frac{\pi}{B_\varepsilon + \ln\left(1 + \frac{1}{\varepsilon^2}\right)}. \tag{29}$$

Here, $B_\varepsilon = (1/\varepsilon)[\pi - 2\tan^{-1}(1/\varepsilon)]$. This expressions hold for the whole frustrated NAF region $-\pi/2 < \phi < 0.15\pi$. It is useful to derive the approximate expression (except very close to $J_1 = 2J_2$) for the extreme quasi-2D case with $\varepsilon^2 \ll 1$. We

obtain

$$k_B T_N \approx (J_1 - 2J_2)\frac{\pi}{2 + \ln\left(\frac{J_1 - 2J_2}{J_\perp}\right)}. \quad (30)$$

For $\varepsilon^2 < 0.1$, this is indistinguishable from Eq. (29).

We note that the natural exchange scale that determines T_N is really $\tilde{J}$ rather than J_c. The sign of $\tilde{J}$ changes at the NAF/CAF boundary and in the CAF phase it simply has to be replaced with $|\tilde{J}|$. Using the (3D) ordering vectors $\mathbf{Q}_{NAF} = (\pi,\pi,\pi)$ and $\mathbf{Q}_{CAF} = (\pi,0,\pi)$ and Eq. (3) we may also express it as

$$\tilde{J} = J_1 - 2J_2 = \tfrac{1}{2}(J_{\mathbf{Q}_{CAF}} - J_{\mathbf{Q}_{NAF}}). \quad (31)$$

For the unfrustrated ($J_2 = 0$) NAF, Eq. (29) reduces to the known result [9]

$$k_B T_N = \frac{\pi J_1}{2 + \ln\left(\frac{J_1}{J_\perp}\right)}. \quad (32)$$

This means the asymptotic $\varepsilon^2 \ll 1$ expression for the frustrated NAF in Eq. (29) can be obtained from the expression for the pure NAF by substituting $J_1 \to \tilde{J}$, i.e., the NN exchange with the effective exchange of the frustrated NAF.

B. CAF structure ($2J_2 > J_1$)

This phase breaks the fourfold in-plane symmetry, therefore, the expanded dispersion $E_{\mathbf{k}}$ is not rotationally symmetric in $\mathbf{k}_\parallel = (k_x,k_y)$. This leads to some complication because $E_{\mathbf{k}}^2$ in Eq. (27) will now depend also on φ, the azimuthal angle in $\mathbf{k}_\parallel = (k_\parallel \cos\varphi, k_\parallel \sin\varphi)$ instead of only on $k_\parallel$ as in the NAF phase [Eq. (28)]. Therefore, a final integration over φ will remain. Furthermore, the cutoff $k_\parallel^c$ has to be chosen such that in the CAF case $J_1 = 0$ which is equivalent to two decoupled interpenetrating NAF sublattices with lattice constant $\sqrt{2}a$ the same T_N as in the previous NAF case with $J_2 = 0$ is obtained. Therefore, $k_\parallel^c = \pi/\sqrt{2}$ must now be chosen. The expansion and integration in Eq. (27) then leads to

$$k_B T_N = (2J_2 - J_1)\frac{\pi}{\frac{2}{\pi}\int_0^\pi d\varphi \frac{1}{b_\varphi^2}\left[B_{\varepsilon\varphi} + \ln\left(1 + \frac{b_\varphi^2}{2\varepsilon^2}\right)\right]}, \quad (33)$$

where we defined

$$b_\varphi^2 = (2J_2 - J_1\cos 2\varphi)/(2J_2 - J_1),$$
$$B_{\varepsilon\varphi} = \frac{b_\varphi}{\sqrt{2}\varepsilon}\left(\pi - 2\tan^{-1}\frac{b_\varphi}{\sqrt{2}\varepsilon}\right), \quad (34)$$

now with $\varepsilon^2 = J_\perp/|\tilde{J}| = J_\perp/(2J_2 - J_1)$. There is no simple general limiting expression for $\varepsilon^2 \ll 1$. For the special case $J_1 = 0$ the model consists of two decoupled NAF substructures. Then, $2\varepsilon^2 = J_\perp/J_2$, $b_\varphi^2 = 1$ and in the extreme quasi-2D case $\varepsilon^2 \ll 1$ we recover Eq. (32) now with the replacement $J_1 \to J_2$.

As stressed before, these expressions contain implicitly an arbitrary momentum cutoff (chosen as zone boundary wave number) on which the absolute value of T_N will depend. In the previous numerical results, on the other hand, the energy cutoff is given naturally by the spin-wave bandwidth. Therefore, it is reasonable to compare T_N and f normalized to the unfrustrated NAF case $\phi = 0$ for the two methods. For small $J_\perp/J_c$ gives a quite satisfactory agreement for all frustration angles ϕ as shown in Fig. 9.

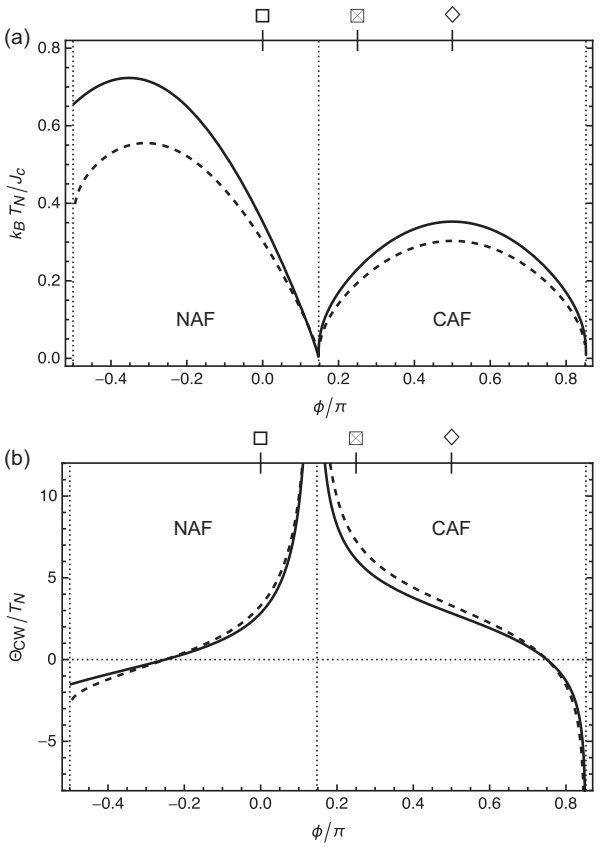

FIG. 9. Comparison of square lattice T_N and $f = \Theta_{CW}/T_N$ using numerical findings from Eq. (27) (dashed lines) and analytical results [Eqs. (29) and (33)] (full lines) results for $J_\perp/J_c = 0.001$.

VII. QUASI-2D H-T PHASE DIAGRAM AND REENTRANCE BEHAVIOR

The ordered moment in the whole frustrated region is reduced from its classical value $m_{\mathbf{Q}} = S$ by a considerable amount (e.g., $0.606S$ in the pure Néel case of the square lattice) [19,20]. It was shown before, using LSW and ED approaches [41], that the application of a magnetic field strongly reduces the quantum fluctuations. Therefore, initially, for a small applied field $B = \mu_0 H$ the ordered moment increases, and on approaching the saturation field H_s decreases again due to the classical geometric canting effect, leading to a nonmonotonic behavior of $m_{\mathbf{Q}}(H)$ which was observed [42] and explained [41] for the quasi-2D $S = \frac{1}{2}$ quantum magnet $Cu(pz)_2(ClO_4)_2$ [43].

The nonmonotonic behavior of $m_{\mathbf{Q}}(H)$ is most pronounced for strong frustration, i.e., when the initial value $m_{\mathbf{Q}}(0)$ is strongly suppressed. A complementary effect is seen in the field dependence of the ordering temperature $T_N(H)$ [42]. For small fields $H \ll H_s$ it was shown to increase [41], again due to the reduction of quantum fluctuations by the applied field. For larger fields approaching the saturation value H_s, $T_N(H)$ eventually has to vanish. Thus, due to the initial increase of $T_N(H)$, a

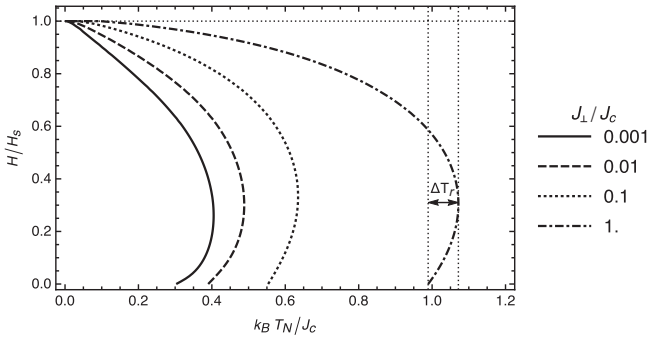

FIG. 10. Field dependence of T_N for pure quasi-2D NAF ($J_2 = 0$) for various interlayer coupling strengths $J_\perp/J_c$ as obtained from Eq. (26). For $J_\perp/J_c = 1$, the absolute reentrance difference ΔT_r (see text) is indicated by the small horizontal double arrow at H_{max}.

reentrance behavior of the magnetic order as function of the applied field at constant temperature $T > T_N^0$ has to be expected.

The full phase diagram for all fields and frustration ratios of a quasi-2D magnet is investigated in the present section. It is obtained from the iterative solution of Eq. (26) which provides us with the phase boundary $T_N(H)$ for the quasi-2D magnet for all parameter sets $(\phi, J_\perp/J_c)$. First, we consider the pure Néel case ($\phi = 0$) shown in Fig. 10. The reentrance behavior caused by the field dependence of quantum fluctuations is clearly seen. The absolute reentrance difference of maximum and zero-field ordering temperature $\Delta T_r = T_N^{max}(H_{max}) - T_N^0$ is rather independent of the 2D character. However, the relative difference $\delta T_r = \Delta T_r/T_N^0 = T_N^{max}/T_N^0 - 1$ which is a measure for the prominence of reentrance in the transition line increases with decreasing $J_\perp/J_c$.

In the complementary Fig. 11 we show the frustration (ϕ) dependence of the transition line for an intermediate 2D character with $J_\perp/J_c = 0.01$. Close to the NAF/FM boundary $\phi/\pi = -0.49$ where quantum fluctuations are strongly reduced, the reentrance behavior characterized by δT_r vanishes. It increases rapidly in the whole unfrustrated $\phi < 0$ regime which proves that the reentrance is primarily associated with the field-dependent suppression of quantum fluctuations and not so much with the effect of frustration. It does, however, achieve a maximum on approaching the strongly frustrated

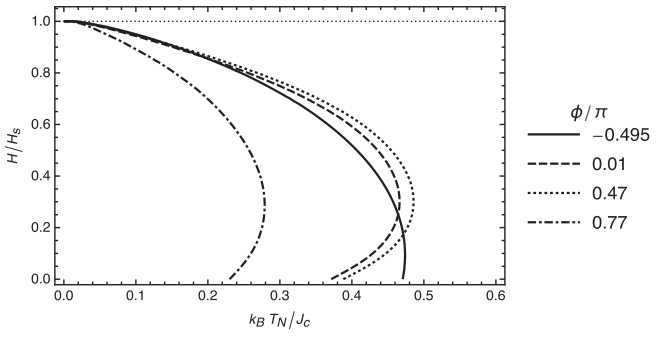

FIG. 11. Field dependence of T_N for interlayer coupling strength $J_\perp/J_c = 0.01$ and various ϕ values corresponding to NAF/FM boundary (full line) and various compound values listed in Table II. The former shows no reentrance due to absence of quantum fluctuations for $\phi/\pi \simeq -0.5$.

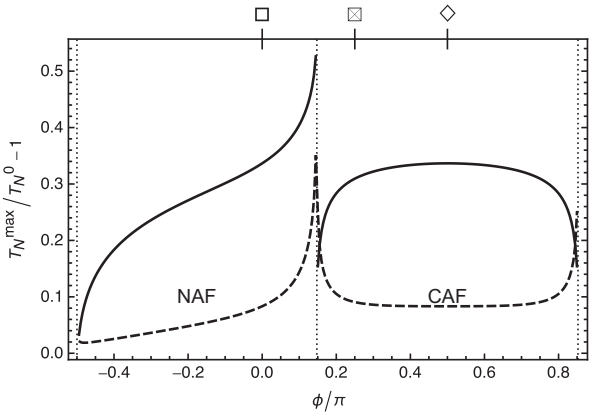

FIG. 12. Reentrance measure given by the difference between the field-dependent maximal Néel temperature and its zero-field value normalized to the latter $\delta T_r = T_N^{max}/T_N^0 - 1$ versus frustration angle ϕ for interlayer coupling strengths $J_\perp/J_c = 0.001$ (solid line) and $J_\perp/J_c = 1$ (dashed line).

regime $\phi/\pi = 0.15$. This is most clearly seen when we plot the reentrance measure δT_r as function of ϕ (Fig. 12) for extreme 2D case (full line) and isotropic 3D case (dashed line). In the NAF case indeed δT_r increases monotonically from NAF/FM ($\phi/\pi = -0.5$) to NAF/CAF ($\phi/\pi = 0.15$) boundaries. In the main part of the CAF phase it stays almost at constant value equal to that of the unfrustrated case. Generally, δT_r is much larger in the extreme quasi-2D magnet (full line) for both phases. Interestingly, in this case the reentrance measure decreases when approaching the strongly frustrated phase boundaries from the CAF side.

VIII. APPLICATION TO QUASI-2D OXOVANADATE COMPOUNDS

The discovery of two classes of layered vanadium oxides Li_2VOXO_4 (X = Si,Ge) [4,5,50,51] and $AA'VO(PO_4)_2$ (A, A' = Pb,Zn,Sr,Ba) [6,7,49,52] provided a variable platform of 2D frustrated quantum magnets with different chemical composition. Nevertheless, their magnetism is described universally by the J_1-J_2 model with J_2/J_1 or ϕ depending on the specific compound. Each of them features V^{4+} ions with $S = \frac{1}{2}$ surrounded by oxygen polyhedra, forming layers of J_1-J_2 square lattices with weak interlayer coupling [7,51].

These compounds were experimentally investigated, e.g., in Refs. [6,45,46] using susceptibility and specific-heat measurements as well as neutron diffraction as tools. The typical observed signatures in these experiments point to quasi-2D magnetism. However, the actual size of $J_\perp/J_c$, i.e., the interlayer/intralayer exchange ratio has not been estimated because an applicable theory for $T_N(\phi, J_\perp)$ for all ϕ was lacking. Using the theoretical results of the previous sections, we can now give an assessment of the size of $J_\perp$ within the series. As input, we use the J_1 and J_2 values obtained previously from 2D finite-temperature Lanczos method (FTLM) applied to the experimental susceptibilities or neutron diffraction results [20] and the experimental values of T_N listed among other items in Table II.

Such a thermodynamic analysis can give only some estimated range of $J_\perp/J_c$ because, on the one hand, the

TABLE II. Exchange interaction constants for various vanadium oxide compounds, ordered with increasing ϕ, i.e., approaching the CAF/FM boundary. Results are obtained mostly from susceptibility $\chi(T)$ and magnetization $m_0(h)$ analysis, except for the fourth and fifth rows which are deduced from neutron diffraction. Here, $\Theta_{\rm CW} = (J_1 + J_2)/k_{\rm B}$ is the 2D Curie-Weiss temperature, $T_{\rm N}$ the Néel temperature, and f the empirical frustration ratio. The symbols in the last column are used in Fig. 13 to label the $k_{\rm B}T_{\rm N}/J_{\rm c}$ data points shown there. The example of $Pb_2VO(PO_4)_2$ shows that a certain variation in exchange parameters as determined by different methods and in different references occurs.

Compound	ϕ/π	$J_{\rm c}/(k_{\rm B}{\rm K})$	$J_1/(k_{\rm B}{\rm K})$	$J_2/(k_{\rm B}{\rm K})$	$\lvert\tilde{J}\rvert/(k_{\rm B}{\rm K})$	$\Theta_{\rm CW}/{\rm K}$	$T_{\rm N}/{\rm K}$	$k_{\rm B}T_{\rm N}/J_{\rm c}$	$k_{\rm B}T_{\rm N}/\lvert\tilde{J}\rvert$	f	Ref.	Symbol
$Zn_2VO(PO_4)_2$	0.008	7.9	7.91	0.2	7.5	8.11	3.7	0.46	0.49	2.19	[7]	•
Li_2VOGeO_4	0.44	4.2	0.82	4.1	7.38	4.92	2.1	0.50	0.28	2.34	[6,44]	△
Li_2VOSiO_4	0.47	6.3	0.56	6.3	12.04	6.86	2.7	0.43	0.22	2.54	[6,44]	△
$Pb_2VO(PO_4)_2$	0.60	6.8	–2	6.5	16.25	4.5	3.5	0.51	0.21	1.28	[45]	♦
$Pb_2VO(PO_4)_2$	0.63	8.4	−3.2	7.7	18.8	4.5	3.7	0.44	0.20	1.22	[46]	♦
$PbZnVO(PO_4)_2$	0.65	11.27	−5.2	10.0	25.2	4.8	3.9	0.35	0.15	1.23	[47]	□
$Na_{1.5}VO(PO_4)_2F_{0.5}$	0.65	7.1	−3.2	6.3	15.8	3.1	2.6	0.36	0.16	1.19	[48]	□
$BaZnVO(PO_4)_2$	0.66	10.5	−4.99	9.26	23.5	4.27	3.8	0.36	0.16	1.12	[44]	□
$Pb_2VO(PO_4)_2$	0.66	10.7	−5.1	9.4	23.9	4.3	3.7	0.35	0.15	1.16	[48]	♦
$Pb_2VO(PO_4)_2$	0.67	11.5	–6	9.8	25.6	3. 8	3.7	0.32	0.14	1.02	[6]	♦
$SrZnVO(PO_4)_2$	0.73	12.2	−8.3	8.9	26.1	0.6	2.7	0.22	0.10	0.22	[48]	□
$BaCdVO(PO_4)_2$	0.77	4.8	−3.6	3.2	10.0	−0.4	1.0	0.21	0.10	−0.4	[48,49]	□

experimental value of $k_{\rm B}T_{\rm N}/J_{\rm c}$ may be rather uncertain. For example for $Pb_2VO(PO_4)_2$, it varies between 0.32 and 0.51 (♦ in Table II). On the other hand, the Néel temperature depends only logarithmically on $J_\perp$ [Eqs. (29) and (33)] and therefore a wide range of values for $J_\perp/J_{\rm c}$ is possible. We plot the experimental values of $k_{\rm B}T_{\rm N}/J_{\rm c}$ from Table II together with two theoretical curves in Fig. 13. The experimental values all lie in a corridor limited by the theoretical results for $J_\perp/J_{\rm c} = 0.1$ (full line) and $J_\perp/J_{\rm c} = 0.001$ (dashed line). We conclude that the oxovanadate series are indeed quasi-2D magnets but with non-negligible interlayer coupling.

The field dependence of the Néel temperature caused by the suppression of fluctuations is discussed in Sec. VII. In the example of $Cu(pz)_2(ClO_4)_2$ [41,42] it was observed and calculated. However, due to the rather high exchange energy scale $J_{\rm c}/k_{\rm B} = 18.6$ K the field for the maximum Néel temperature $T_{\rm N}^{\rm max}(H)$ is not reached such that the phase diagram with reentrance character, although certainly present, has not been fully determined.

A more favorable case is $Pb_2VO(PO_4)_2$ [44]. The smaller exchange energy scale (Table II) makes it possible to reach $T_{\rm N}^{\rm max}(H) \approx 3.9$ K at $\mu_0 H \approx 8$ T in susceptibility and specific-heat measurements [6]. At the largest accessible field $\mu_0 H = 14$ T the $T_{\rm N}(H)$ curve has started to turn back. The experimental values together with the optimal theoretical curve for $J_\perp/J_{\rm c} = 0.02$ and $\phi/\pi = 0.63$ appropriate for $Pb_2VO(PO_4)_2$ are plotted in Fig. 14.

The fitting of the whole $T_{\rm N}(H)$ curve leads to a more reliable value for $J_\perp$ than just comparing $T_{\rm N}^0$ as in Fig. 13. The observed experimental reentrance behavior is somewhat less pronounced than expected for these parameters. One reason certainly is that $Pb_2VO(PO_4)_2$ has a small Ising anisotropy that suppresses part of the fluctuations and therefore $T_{\rm N}^0$ is less reduced by quantum fluctuations than in the pure isotropic Heisenberg case. The presence of this Ising term may be concluded from a spin-flop transition below $\mu_0 H_{\rm sf} \approx 0.9$ T not shown in the data of Fig. 14.

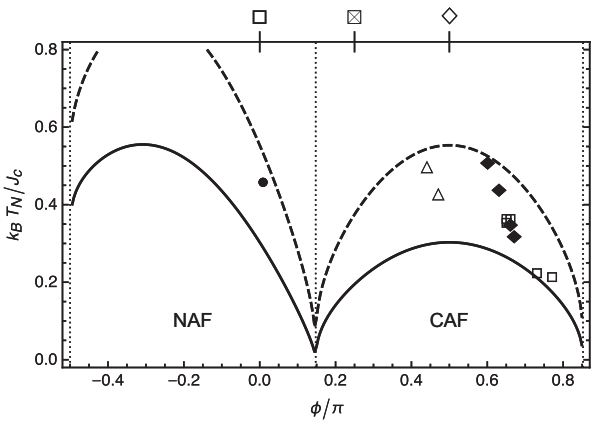

FIG. 13. Néel temperature $T_{\rm N}$ versus frustration angle ϕ. Dots: experimental values according to Table II. Lines from evaluation of Eq. (27) for $J_\perp/J_{\rm c} = 0.001$ (full line) and 0.1 (dashed line).

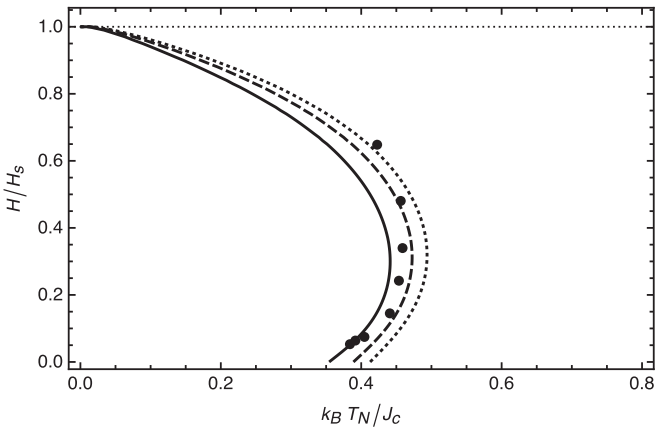

FIG. 14. Reentrance behavior of $T_{\rm N}(H)$ in $Pb_2VO(PO_4)_2$ [44] (black dots). Good agreement is obtained for $J_\perp/J_{\rm c} = 0.02$ (dashed line) using $\phi/\pi = 0.63$ and $J_{\rm c} = 8.4\,{\rm K}/k_{\rm B}$ from Table II and a saturation field $\mu_0 H = 20.9$ T [20]. Full and dotted curves correspond to values $J_\perp/J_{\rm c} = 0.01, 0.03$, respectively.

In any case, one may expect that reentrant behavior is a ubiquitous phenomenon for quasi-2D quantum magnets due to the universal mechanism of suppressing quantum fluctuations by application of the field. This mechanism is also obvious from the temperature dependence of the specific heat, for example, in $Pb_2VO(PO_4)_2$ which shows an increasing sharpening of the transition peak for increasing field [44] due to the suppression of spin fluctuations, a very typical behavior for reentrant phase transitions. The present theory may also be applied to study this effect.

IX. DISCUSSION AND SUMMARY

We have investigated the frustration, interlayer coupling, and field dependence of the Néel temperature in quasi-2D quantum magnets. Based on the simple Tyablikov self-consistency modification of LSW theory we have derived equations that should qualitatively describe the systematic variation of T_N with frustration parameter $\phi = \tan^{-1}(J_2/J_1)$, interlayer coupling $J_\perp$, and the applied field H up to the saturation value H_s. Furthermore, we investigated to what extent the experimentally used empirical frustration ratio $f = \Theta_{CW}/T_N$ (which may be positive or negative) is a relevant measure of frustration. In the mean field approximation, $|f|$ is of order one or less.

We find that indeed the Néel temperature $T_N(\phi)$ is strongly suppressed for regions with large frustration and accordingly $|f|$ may be greatly enhanced in narrow intervals around these special points with $|2J_2/J_1| = 1$ or $\phi/\pi \approx 0.15, 0.85$ where the ground-state magnetic moment breaks down and spin liquid or spin nematic states [20] are established. In these regions, $|f| \gg 1$ can function as a useful measure of frustration, in particular in the square lattice (Fig. 7). The logarithmic dependence of T_N on interlayer coupling $J_\perp$ for the unfrustrated case $J_2 = 0$ is confirmed to hold in both NAF and CAF sectors for all frustration degrees. This is also proven by explicit analytical approximations for $T_N(\phi)$.

However, our analysis shows that the criterion $|f| \gg 1$ as an indicator for large frustration may also be misleading. Especially in the anisotropic triangular lattice (Fig. 8) the criterion is also fulfilled for the *unfrustrated* quasi-1D cases with $\phi/\pi = \pm 0.5$, being far away from the special regions of strong frustration with $\phi/\pi \approx 0.15$ and 0.85 (see Fig. 2). Instead, critical 1D fluctuations lead to the enhancement of f here. Particular examples are the well-known anisotropic triangular magnets $CsCuCl_4$ ($f = 5.6$) and $CsCuBr_4$ ($f = 9.2$). They have strongly enhanced f values, but anisotropy parameters $\phi/\pi = 0.41$ and 0.38, respectively [3,53,54]. Although they are still quasi-2D magnets with finite T_N of 0.62 and 1.42 K, respectively, they are already placed close to the quasi-1D region of the phase diagram with interchain couplings $J_1/J_2 \approx 0.29$ and 0.40 and rather reduced frustration degree (Fig. 2). That quasi-1D fluctuations are the reason for large-f values in these compounds is also directly evident from the typical quasi-1D spinon excitation continuum observed in inelastic neutron scattering experiments [53].

Furthermore, the large family of square-lattice oxovanadate quasi-2D magnets with one exception have frustration angles in the interval $0.44 < \phi/\pi < 0.77$. This begins close to the unfrustrated CAF and ends before the strongly frustrated CAF region slightly below $\phi/\pi \approx 0.85$. Therefore, the values of $|f|$ in this family of compounds are rather close to one (Table II) without dramatic variation.

In essence then, be it the square or anisotropic triangular lattice, in order to use the size of $f = \Theta_{CW}/T_N$ as a frustration criterion for a compound investigated, one should have additional information beforehand about its location in the phase diagram. This can, for example, be the determination of ϕ by a FTLM fit to the temperature dependence of the magnetic susceptibility.

We have analyzed the field dependence of the Néel temperature and found it is determined by the universal effect of reduction of moment fluctuations by the applied field. It is known that this mechanism leads to a nonmonotonic field dependence of the ordered moment [41,42]. The present analysis has shown that it also leads to a nonmonotonic $T_N(H)$ behavior, i.e., a reentrance character of the H-T phase diagram in quantum magnets. The quantity $\delta T_r = \Delta T_r/T_N^0 = T_N^{max}/T_N^0 - 1$ characterizing the reentrance shows a pronounced dependence on frustration angle in the strongly frustrated regimes around the classical phase boundaries NAF/CAF and CAF/FM. Outside these regions, it increases strongly with decreasing $J_\perp$ on approaching the extreme quasi-2D limit.

Such reentrance phase diagrams as in Figs. 11 and 14 should therefore be ubiquitous among quasi-2D magnets but may not always easily be observable in the experimentally available range of magnetic fields. The oxovanadate $Pb_2VO(PO_4)_2$ is an exception where reentrance has been found due to a modest estimated saturation field $\mu_0 H_s \approx 20.9$ T, a consequence of the relatively small exchange constants J_1 and J_2 of the material (see Table II). $T_N(H)$ follows qualitatively the expected behavior, however, the details may be subject to exchange anisotropies not taken into account here and further interactions which influence zero-field spin fluctuations and thus modify the zero-field value T_N^0. The inclusion of such effects in the present framework via modified spin-wave excitations seems rather straightforward.

ACKNOWLEDGMENT

We would like to thank Ch. Geibel for discussion and the permission to use unpublished data.

APPENDIX A: GLOBAL AND LOCAL SPIN COORDINATES IN A MAGNETIC FIELD

The spin-wave approximation is performed in a coordinate system where the local z direction at a given site i coincides with the moment direction at that site. The connection to the global spin coordinates used in Eq. (1) is given by

$$\begin{pmatrix} S_i^x \\ S_i^y \\ S_i^z \end{pmatrix} = \begin{pmatrix} \cos(\mathbf{QR}_i) & -\sin(\mathbf{QR}_i) & 0 \\ \sin(\mathbf{QR}_i) & \cos(\mathbf{QR}_i) & 0 \\ 0 & 0 & 1 \end{pmatrix} \times \begin{pmatrix} \cos\Theta & 0 & \sin\Theta \\ 0 & 1 & 0 \\ -\sin\Theta & 0 & \cos\Theta \end{pmatrix} \begin{pmatrix} S_i^{x'} \\ S_i^{y'} \\ S_i^{z'} \end{pmatrix}. \quad \text{(A1)}$$

For clarity, we denote the local spin coordinates with primes in this expression. While the first matrix represents the in-plane xy rotation due to spontaneous order characterized by $\mathbf{Q}$, the second one describes the xz-plane canting of spins with angle Θ caused by the magnetic field with a classical value $\cos\Theta_{\rm cl} = H/H_{\rm s}$.

APPENDIX B: EXPANSION INTEGRALS FOR THE ORDERED MOMENT

In zero field for $T \leqslant T_{\rm N}$ the approximate solution for the total moment $\langle S\rangle$ in Eq. (25) is determined by expansion coefficients that are expressed in terms of frustration- (ϕ-) dependent integrals $I_0 \ldots I_2$. They are given by

$$I_0 := \frac{1}{3}\int_{\rm BZ}\frac{d^3k}{V_{\rm BZ}}(A_{\mathbf{k}} - B_{\mathbf{k}}\cos\Theta_{\rm cl}), \tag{B1}$$

$$I_1 := \frac{1}{180}\int_{\rm BZ}\frac{d^3k}{V_{\rm BZ}}(A_{\mathbf{k}} - B_{\mathbf{k}}\cos\Theta_{\rm cl})E_{\mathbf{k}}^2, \tag{B2}$$

$$I_2 := \frac{1}{7560}\int_{\rm BZ}\frac{d^3k}{V_{\rm BZ}}(A_{\mathbf{k}} - B_{\mathbf{k}}\cos\Theta_{\rm cl})E_{\mathbf{k}}^4. \tag{B3}$$

Using these integrals in Eq. (25) leads to the approximate $\langle S\rangle(T)$ curves in Fig. 4.

APPENDIX C: NÉEL TEMPERATURE AT THE CAF BORDERS

From Eq. (27), we obtain

$$\begin{aligned}\beta_{\rm N} &= 4\int_{\rm BZ}\frac{d^3k}{V_{\rm BZ}}\frac{A_{\mathbf{k}}}{A_{\mathbf{k}}^2 - B_{\mathbf{k}}^2}\\ &= 2\int_{\rm BZ}\frac{d^3k}{V_{\rm BZ}}\left(\frac{1}{A_{\mathbf{k}} - B_{\mathbf{k}}} + \frac{1}{A_{\mathbf{k}} + B_{\mathbf{k}}}\right)\\ &= 4\int_{\rm BZ}\frac{d^3k}{V_{\rm BZ}}\frac{1}{A_{\mathbf{k}} + B_{\mathbf{k}}},\end{aligned} \tag{C1}$$

where the last equality holds for commensurate ordering vectors $\mathbf{Q}$ with components $(Q_x,Q_y,Q_z) = \pi(n_x,n_y,n_z)$ and $n_x,n_y,n_z \in \mathbb{Z}$. At the CAF borders, we have either $J_2 = J_1/2$ (border to NAF) or $J_2 = -J_1/2 > 0$ (border to FM) such that we obtain from Eq. (17)

$$A_{\mathbf{k}} + B_{\mathbf{k}} = 2[J_1(1+\cos k_x)(1+\cos k_y) + J_\perp(1+\cos k_z)] \tag{C2}$$

at the NAF/CAF border and a similar expression at the FM/CAF border. The denominator in Eq. (C1) therefore has lines of zeros at $(k_x,k_y,k_z) = (\pi,k_y,\pi)$ or $(k_x,k_y,k_z) = (k_x,\pi,\pi)$, implying that the integral (C1) diverges and $T_{\rm N} \to 0$ eventually.

[1] D. C. Mattis, *The Theory of Magnetism Made Simple* (World Scientific, Singapore, 2006).
[2] N. Shannon, B. Schmidt, K. Penc, and P. Thalmeier, Eur. Phys. J. B **38**, 599 (2004).
[3] B. Schmidt and P. Thalmeier, New J. Phys. **17**, 073025 (2015).
[4] R. Melzi, P. Carretta, A. Lascialfari, M. Mambrini, M. Troyer, P. Millet, and F. Mila, Phys. Rev. Lett. **85**, 1318 (2000).
[5] P. Carretta, N. Papinutto, R. Melzi, P. Millet, S. Gonthier, P. Mendels, and Pawel Wzietek, J. Phys.: Condens. Matter **16**, S849 (2004).
[6] E. E. Kaul, H. Rosner, N. Shannon, R. V. Shpanchenko, and C. Geibel, J. Magn. Magn. Mater. **272**, 922 (2004).
[7] N. S. Kini, E. E. Kaul, and C. Geibel, J. Phys.: Condens. Matter **18**, 1303 (2006).
[8] T. Thio, T. R. Thurston, N. W. Preyer, P. J. Picone, M. A. Kastner, H. P. Jenssen, D. R. Gabbe, C. Y. Chen, R. J. Birgeneau, and A. Aharony, Phys. Rev. B **38**, 905 (1988).
[9] N. Majlis, S. Selzer, and G. C. Strinati, Phys. Rev. B **45**, 7872 (1992).
[10] C. Yasuda, S. Todo, K. Hukushima, F. Alet, M. Keller, M. Troyer, and H. Takayama, Phys. Rev. Lett. **94**, 217201 (2005).
[11] S. V. Tyablikov, *Methods in the Quantum Theory of Magnetism* (Springer, Boston, MA, 1967).
[12] D. A. Yablonskiy, Phys. Rev. B **44**, 4467 (1991).
[13] N. Majlis, S. Selzer, and G. C. Strinati, Phys. Rev. B **48**, 957 (1993).
[14] V. Y. Irkhin and A. A. Katanin, Phys. Rev. B **55**, 12318 (1997).
[15] D. Ihle, C. Schindelin, A. Weiße, and H. Fehske, Phys. Rev. B **60**, 9240 (1999).
[16] A. Katanin, Phys. Rev. B **86**, 224416 (2012).
[17] S. C. Furuya, M. Dupont, S. Capponi, N. Laflorencie, and T. Giamarchi, Phys. Rev. B **94**, 144403 (2016).
[18] M. Härtel, J. Richter, D. Ihle, and S.-L. Drechsler, Phys. Rev. B **81**, 174421 (2010).
[19] B. Schmidt, M. Siahatgar, and P. Thalmeier, Phys. Rev. B **83**, 075123 (2011).
[20] B. Schmidt and P. Thalmeier, Phys. Rep. **703**, 1 (2017).
[21] In this and all other multipart figures, we use the convention that panels are labeled a, b, c, ... from left to right and/or from top to bottom.
[22] B. Schmidt and P. Thalmeier, Phys. Rev. B **89**, 184402 (2014).
[23] O. A. Starykh, Rep. Prog. Phys. **78**, 052502 (2015).
[24] L. Savary and L. Balents, Rep. Prog. Phys. **80**, 016502 (2017).
[25] Weihong Zheng, R. H. McKenzie, and R. R. P. Singh, Phys. Rev. B **59**, 14367 (1999).
[26] S. Yunoki and S. Sorella, Phys. Rev. B **74**, 014408 (2006).
[27] M. Q. Weng, D. N. Sheng, Z. Y. Weng, and R. J. Bursill, Phys. Rev. B **74**, 012407 (2006).
[28] D. Heidarian, S. Sorella, and F. Becca, Phys. Rev. B **80**, 012404 (2009).
[29] P. Hauke, T. Roscilde, V. Murg, J. I. Cirac, and R. Schmied, New J. Phys. **12**, 053036 (2010).
[30] H.-C. Jiang, H. Yao, and L. Balents, Phys. Rev. B **86**, 024424 (2012).
[31] L. Siurakshina, D. Ihle, and R. Hayn, Phys. Rev. B **61**, 14601 (2000).
[32] X. Obradors, A. Labarta, A. Isalgué, J. Tejada, J. Rodriguez, and M. Pernet, Solid State Commun. **65**, 189 (1988).
[33] A. P. Ramirez, Annu. Rev. Mater. Sci. **24**, 453 (1994).

[34] B. Wilfong, X. Zhou, H. Vivanco, D. J. Campbell, K. Wang, D. Graf, J. Paglione, and E. Rodriguez, arXiv:1711.06725.
[35] Indeed for ferromagnets, $|\Theta_{CW}|$ is identical to the mean-field Curie temperature T_c.
[36] M. E. Zhitomirsky and A. L. Chernyshev, Rev. Mod. Phys. **85**, 219 (2013).
[37] B. Schmidt, M. Siahatgar, and P. Thalmeier, Phys. Rev. B **81**, 165101 (2010).
[38] A. L. Chernyshev and M. E. Zhitomirsky, Phys. Rev. B **79**, 144416 (2009).
[39] V. N. Kotov, J. Oitmaa, O. P. Sushkov, and Z. Weihong, Phys. Rev. B **60**, 14613 (1999).
[40] Note that in this work the T_N curves are resulting from the condition of vanishing order parameter which is calculated in selfconsistent TA approach, whereas in Ref. [10] T_N is obtained from the condition of the divergent RPA susceptibility of a quasi-2D Néel antiferromagnet ($J_2 = 0$) above T_N.
[41] M. Siahatgar, B. Schmidt, and P. Thalmeier, Phys. Rev. B **84**, 064431 (2011).
[42] N. Tsyrulin, F. Xiao, A. Schneidewind, P. Link, H. M. Rønnow, J. Gavilano, C. P. Landee, M. M. Turnbull, and M. Kenzelmann, Phys. Rev. B **81**, 134409 (2010).
[43] N. Tsyrulin, T. Pardini, R. R. P. Singh, F. Xiao, P. Link, A. Schneidewind, A. Hiess, C. P. Landee, M. M. Turnbull, and M. Kenzelmann, Phys. Rev. Lett. **102**, 197201 (2009).
[44] E. E. Kaul, Experimental Investigation of New Low-Dimensional Spin Systems in Vanadium Oxides, Ph.D. thesis, Technische Universität Dresden, 2005.
[45] M. Skoulatos, J. P. Goff, N. Shannon, E. E. Kaul, C. Geibel, A. P. Murani, M. Enderle, and A. R. Wildes, J. Magn. Magn. Mater. **310**, 1257 (2007).
[46] M. Skoulatos, J. P. Goff, C. Geibel, E. E. Kaul, R. Nath, N. Shannon, B. Schmidt, A. P. Murani, P. P. Deen, M. Enderle, and A. R. Wildes, Europhys. Lett. **88**, 57005 (2009).
[47] A. A. Tsirlin, R. Nath, A. M. Abakumov, R. V. Shpanchenko, C. Geibel, and H. Rosner, Phys. Rev. B **81**, 174424 (2010).
[48] A. A. Tsirlin, B. Schmidt, Y. Skourski, R. Nath, C. Geibel, and H. Rosner, Phys. Rev. B **80**, 132407 (2009).
[49] R. Nath, A. A. Tsirlin, H. Rosner, and C. Geibel, Phys. Rev. B **78**, 064422 (2008).
[50] P. Millet and C. Satto, Mater. Res. Bull. **33**, 1339 (1998).
[51] R. Melzi, S. Aldrovandi, F. Tedoldi, P. Carretta, P. Millet, and F. Mila, Phys. Rev. B **64**, 024409 (2001).
[52] R. Nath, Y. Furukawa, F. Borsa, E. E. Kaul, M. Baenitz, C. Geibel, and D. C. Johnston, Phys. Rev. B **80**, 214430 (2009).
[53] R. Coldea, D. A. Tennant, and Z. Tylczynski, Phys. Rev. B **68**, 134424 (2003).
[54] O. A. Starykh, H. Katsura, and L. Balents, Phys. Rev. B **82**, 014421 (2010).